PROPULSION DIVISION

MONITORING OF CRACK GROWTH IN TI-6AL-4V ALLOY BY THE STRESS WAVE ANALYSIS TECHNIQUE

December 1968

AEROJET-GENERAL CORPORATION
SACRAMENTO, CALIFORNIA

MONITORING OF CRACK GROWTH IN TI-6AL-4V ALLOY BY THE STRESS WAVE ANALYSIS TECHNIQUE

by

W. G. Reuter, A. T. Green, C. E. Hartbower, and P. P. Crimmins

December 1968

Prepared Under Contract NAS 9-7759 for
the NASA Manned Spacecraft Center
Houston, Texas

Advanced Materials Technology Section
Research and Technology Department
Aerojet-General Corporation
Sacramento, California

42277T

FOREWORD

This report was prepared by Aerojet-General Corporation, Sacramento, California, under NASA Contract NAS 9-7757, during the period July to December 1968. The work was administered under the direction of Mr. W. L. Castner of the NASA-Manned Spacecraft Center, Houston, Texas.

The study program at the Aerojet-General Corporation was performed under the technical direction of A. T. Green. Aerojet personnel who also participated in the program include W. G. Reuter, Research Engineer, C. E. Hartbower, Fracture Mechanics, and P. P. Crimmins, Manager of Structural Metals Research and Development, Advanced Materials Technology. All of these personnel participated in the preparation of this report.

ABSTRACT

The results of investigations to establish stress-wave analysis technique (SWAT) system parameters for the monitoring of thin walled Ti-6Al-4V pressure vessels such as the Apollo SPS tank are presented. Sensor attachment techniques which overcome previous problems encountered when bonding cement was used to attach the sensor to the test article are described. Stress-wave emission characteristics which can be employed as precursors of failure in air, distilled water inhibited with sodium dichromate (500 ppm) and methyl alcohol environments were determined, and a SWAT system possessing sufficient sensitivity to detect and monitor stress wave emissions associated with subcritical crack growth is discussed. Critical stress intensity data and relationships between applied stress intensity and failure time for the various material thicknesses (0.030 and 0.060-in.) and environments investigated are presented. Application of the results obtained to the proof testing of critical tankage is discussed and recommendations for follow-on studies are presented.

TABLE OF CONTENTS

TABLE LIST

FIGURE LIST

FIGURE LIST (cont.)

I. INTRODUCTION

The reliability and quality assurance of propellant containment tanks in man-rated space vehicles is of paramount importance to NASA. One of the methods employed to ensure maximum reliability in such vessels is the proof test. Experience has shown that proof testing to a level above the tanks operating pressure is generally useful as a quality assurance measure to detect flaws large enough to fail the vessel at or below the operating pressure. However, numerous proof-test failures have occurred during the hold period at maximum pressure which serve as reminders of the danger of subcritical crack growth both during hydrotest and service (due to environmentally-induced growth), and demonstrates the need for a nondestructive inspection technique which can be employed during pressurization to detect the initiation and growth of subcritical defects (Ref 1) and determine their location.

The Aerojet Stress Wave Analysis Technique (SWAT) is an inspection method which promises to meet these requirements. With this technique, transducers are employed to detect the stress-wave emissions, which accompany the energy release occurring when a flaw propagates, and through seismic techniques, triangulate back to the source of the emission. The technique has been employed for this purpose during previous pressure vessel hydrotests (Refs 2 and 3), including the hydroburst (Ref 4) of an Apollo service propulsion system (SPS) fuel tank.

The service history of the SPS tank is of particular interest in connection with this study. The vessel had been removed from Aifframe-017 after its mating fuel tank had ruptured at 240 psig during a system pressure test using methyl alcohol. Following hydroburst, the interior surfaces of the vessel were found to contain many small surface flaws, presumably the result of stress corrosion in the methyl alcohol environment. Although SWAT was successfully employed to detect the onset of failure during the hydroburst of the SPS fuel tank, difficulties were encountered due to cracking of the cement used to

bond the SWAT transducers to the vessel. This difficulty resulted from the high strain occurring in the thin-walled (0.030 to 0.060-in.) SPS tank. Cracking of the bonding cement produced extraneous signals which complicated the SWE data analysis. Also, during this test, relatively few stress waves attributable to flaw growth were observed, suggesting that very small amplitude stress waves were associated with the growth of the surface flaws which had been produced by previous pressurizations in a methyl alcohol environment.

In view of the latter difficulties, the program described herein was undertaken. The objectives of the program were to:

1. Demonstrate improved transducer attachment techniques;
2. To determine stress-wave characteristics associated with part-through flaw growth in the titanium 6Al-4V alloy exposed to air, distilled water inhibited with sodium dichromate, and methyl alcohol environments;
3. Define the system sensitivity required to detect the stress-wave emission sensitivity associated with flaw growth; and
4. Compare and correlate such characteristics with data obtained from the SPS tankage hydroburst previously performed.

II. SUMMARY

Sensor attachment techniques were successfully developed which overcome previous bonding agent cracking encountered during the hydrotest of the SPS tank. The technique recommended for use with pressure vessels incorporates an attachment block to which the sensor is mounted and which, itself, is mounted to the test article using RTV silicon rubber. This technique provides the degree of contact required for good stress-wave emission transmissability, does not produce extraneous signals and will withstand the environmental conditions to which the SPS fuel tank is subjected.

The stress-wave emission characterization studies were performed using Ti-6Al-4V material (0.030 and 0.060-in. thick) supplied by NASA from a discarded SPS tank. The tests were performed using fatigue precracked part-through-crack tensile specimens which were also employed to determine critical stress intensity values. The results obtained indicated K_{Ic} values of 43.5 ksi-in.$^{1/2}$ and 45.9 ksi-in.$^{1/2}$, respectively, for 0.030 and 0.060-in. thick material. These corresponded to a value of 44 ksi-in.$^{1/2}$ obtained by NASA for the same material and was independent of air or inhibited water environment. Critical stress intensity values were not calculated for the methyl alcohol environment tests since specimens tested in this environment always failed during hold and no accurate measurements of the slow crack growth were possible. The failure time in methyl alcohol was dependent on the initial applied stress intensity. Conversely, neither slow crack growth nor specimen failure was observed in air and/or inhibited water environments for hold periods up to 18 hours at applied stress intensity values of up to 0.92 K_{Ic}; failure only occurred during rising load to the K_{Ic} value.

The system sensitivity required to detect stress-wave emissions from subcritical crack growth in thin walled (0.030 and 0.060-in.) 6Al-4V titanium was successfully achieved and demonstrated in air, inhibited water, and methyl alcohol environments. Verification of adequate SWAT-system sensitivity was

made through analysis of stress-wave emission data from a previous Apollo SPS-tank hydroburst.

The stress-wave-emission characteristics which were determined as precursors of failure were the same for all environments investigated; these are: (1) the rate of occurrence, (2) the cumulative count, and (3) the amplitude of stress-wave emissions, all of which increased significantly as failure was approached. In air and inhibited water, no significant SWE were observed under sustained load for hold periods of up to 18 hours. This was consistent with the fact that there was neither evidence of slow crack growth in the fracture surfaces nor failure during the hold periods. Failure during subsequent rising load was detected by monitoring the stress-wave emissions occurring and was attended by increased stress-wave rate of occurrence and amplitude. In methyl alcohol, SWE indicative of the subcritical crack growth were observed during the holding periods and increased both in rate of occurrence and amplitude as failure approached. The interval between the onset of detectable crack growth as shown by the stress-wave emission data and actual failure, varied as a function of environment and applied stress intensity; in all instances, this time interval was sufficient to terminate the pressurizing cycle in a hydrotest prior to failure.

III. TRANSDUCER ATTACHMENT TECHNIQUE

A. BACKGROUND

Prior to the hydroburst of the SPS fuel tank, a wide variety of adhesives had been used for attaching stress-wave sensors to the test item. In addition to adhesives, other sensor fastening techniques including mechanical devices such as wrap-around spring cords or coiled springs, had also been employed. Many of these techniques are currently in use, depending on the specific application and when correctly applied, are acceptable methods. The more important considerations regarding the attachment of the sensor are:

1. The attachment should be as near to being an integral part of the test item as possible.

2. The attaching method must withstand, without failing or cracking, the structural and environmental conditions to which the test object is exposed.

3. The attachment should not change, nor affect the primary structural characteristics of the test item.

4. The attachment assembly should present as small a mechanical impedance as is practically possible. This usually suggests a very stiff attaching method and a very small mass for both sensor and attachment device.

5. The attachment and removal of the sensor should be easily accomplished without excessive preparatory time, and should not require materials, equipment and skills beyond those normally acquired by competent test laboratory personnel.

III, A, Background (cont.)

The attachment procedure previously used to install stress-wave sensors on the SPS fuel tank are described below:

1. The surface of the fuel tank was roughened at each of the sensor locations using a fine grade of sandpaper.

2. The surface was then cleaned with Methyl Ethyl Ketone (MEK).

3. Aluminum alloy attachment blocks (1/2-in. dia x 1/2-in. long, drilled and tapped (10-32) on one side for mounting the sensor) were then sanded and also cleaned with MEK.

4. The attachment blocks were lightly coated with Budd Co. GA-2 epoxy strain gage adhesive and applied to the sensor location on the fuel tank, which had also been lightly coated with the adhesive.

5. A light spring load of 5 lb was used to hold the attachment block in position for approximately 48 hr at ambient conditions while the epoxy adhesive cured.

6. The sensors were then secured to each of the attachment blocks with threaded studs.

Exclusive of the epoxy cure time, the total time required to install the blocks used during testing of the SPS fuel tank was approximately 20 min. The Budd Co. GA-2 epoxy strain gage adhesive had not been used for attaching stress-wave emission sensors prior to the hydrotest of the SPS fuel tank. However, this material was selected since the manufacturer's specification indicated a maximum strain level before cracking of 20%, which was in excess of that anticipated during the burst testing of the SPS tank.

III, A, Background (cont.)

If the strain requirements of the attachment adhesive are considered, the requirement for a high elongation without cracking becomes readily apparent. As shown in Figure 1, when the test specimen elongates to a strain of ΔL, the adhesive joint is strained an equivalent amount in shear because of the stiffness of the attachment block. These shearing strains are considerably higher than with a conventional strain gage because the strain gage movement at the tank wall-attachment block interface very closely matches that of the structure. In situations where the test specimen is in a vertical position, the adhesive joint is also subjected to a bending moment due to the weight of the sensor and attachment block assembly.

Most epoxy adhesives should be capable of remaining intact to and slightly beyond the hydrostatic proof test strain levels usually experienced by aerospace fuel tanks. However, in thin-walled tanks such as the SPS vessel, unusually high strain levels may be encountered and can result in adhesive cracking. In addition, another generally more common mode of adhesive failure is lack of adhesion to one of the bonding surfaces. This can occur because of inadequate cleaning procedures and may be a problem because of the difficulty in completely removing the titanium oxide coating resulting from post-welding stress relieving-aging treatments employed in processing titanium pressure vessels such as the SPS tank.

During this investigation, the cracking of the Budd Co. GA-2 epoxy strain gage adhesive was verified. Tensile specimens supplied by NASA from an SPS chamber, were tested by bending to predetermined strain levels with both stress-wave sensors and strain gages attached. The same sensor attachment techniques used during the SPS fuel tank hydrotest program were employed. During these tests, the stress-wave sensors showed acceleration transients beginning at small deflections; these transients increased as the deflection was increased. Examination of the specimen indicated no flaw interaction or growth, but cracking of the adhesive was observed.

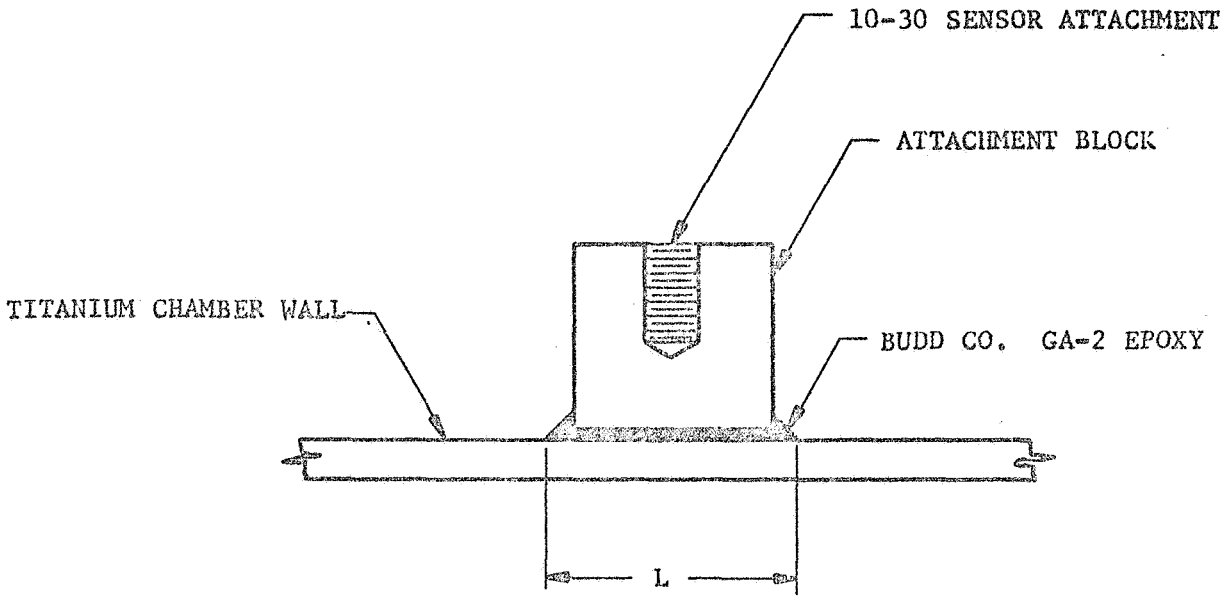

FIGURE 1a

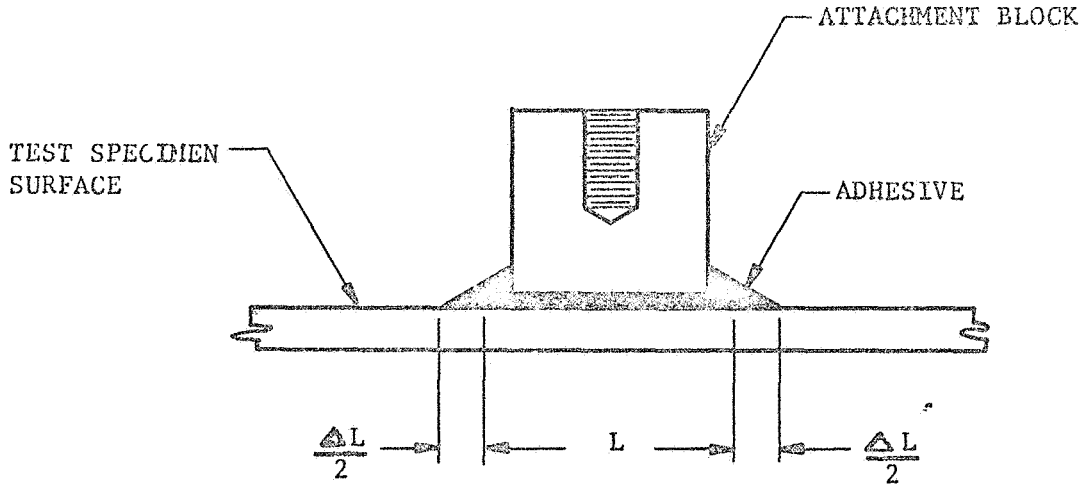

FIGURE 1b

Figure 1. SCHEMATIC REPRESENTATION OF SENSOR ATTACHMENT PROBLEM ENCOUNTERED IN APOLLO SPS TANK HYDROTEST.

III, A, Background (cont.)

A review of signal impedance studies (Refs 5 and 6) indicates that the mounting should be as "stiff" as the structure to which it is attached. If a "softer" technique is employed, signal attenuation occurs because of the "interface" produced between the two components of significantly different moduli. Obviously, then, an attachment technique which employs a welded or threaded connection to which the sensor can be attached and brought to bear directly on the specimen surface would be desirable. However, during the testing of most aerospace pressure vessels, it is not possible to weld or drill and tap to the structure; this is particularly so when testing very thin walled vessels such as the titanium SPS fuel tank. Consequently, an alternate technique required development which would provide adequate contact between the test specimen and sensor without introducing neither a source of extraneous signals nor significant stress-wave attenuation.

B. RECOMMENDED SENSOR ATTACHMENT PROCEDURES

During SWAT tests of Aerojet-fabricated second-stage Minuteman rocket motor cases fabricated using the 6Al-4V titanium alloy (approximately 0.1 in. thick), various sensor attachment techniques were evaluated. The method which was finally selected and used successfully requires a slightly longer preparatory time than the technique previously used, but can be modified slightly to lessen this time. Figure 2 shows a cross-section of the stress-wave emission sensor installation which was established for use on production proof hydrotests of titanium pressure vessels. As recommended in Ref 5, a slight film of light machine oil is also used between the sensor and the test specimen, thereby greatly increasing the transmissability of the signal.

On the basis of the aforementioned effort and the tests conducted during this program, the following procedure has been established for attaching

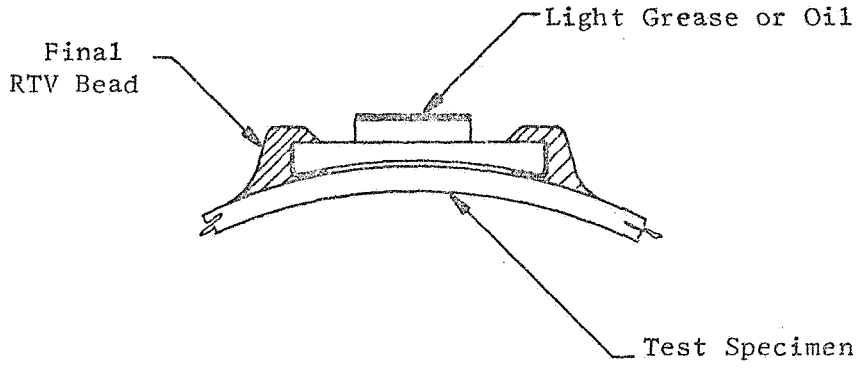

Figure 2. RTV PLACEMENT AFTER POSITIONING ON THE TEST SPECIMEN.

stress-wave-emission sensors to titanium pressure vessels of known dimensions and test pressures.

1. Fabricate an attachment block of the design shown in Figure 3 for each sensor location. This block is to be made of either aluminum or titanium alloy.

2. After accurately marking each sensor location on the test vehicle, thoroughly clean the surface in a circle whose diameter is 1.5 times that of the attachment block. A good cleaning procedure consists of: (a) degreasing the surface with an acceptable solvent for titanium, (b) lightly abrading the surface with a fine grade of emery or sandpaper, and (c) cleaning the surface again with a nonresidue solvent. Care must be taken not to use solvents which can produce corrosion or stress corrosion in the material being tested.

3. Follow the same procedure as 2 above for the base and edges of each attachment block.

4. Lightly precoat both the attachment block and test specimen with the room-temperature vulcanizing (RTV) silicone rubber primer, General Electric No. SS4004, on the areas shown in Figure 4, and allow one hour to dry. Mix the RTV silicone rubber, General Electric No. 60 in accordance with the manufacturer's instruction; 25 gm is adequate for one or two attachment block installations. Apply a very thin layer to the bottom surface of the attachment block over the precoated area. Build up a 1/8 to 1/4-in. bead around the peripheral edge of the block and in contact with that applied to the base.

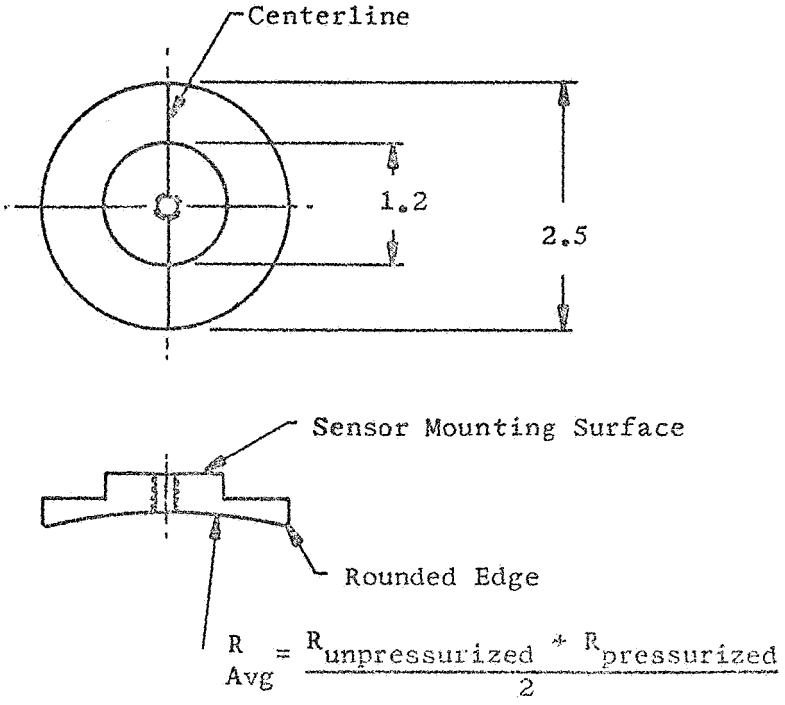

Figure 3. SENSOR ATTACHMENT BLOCK.

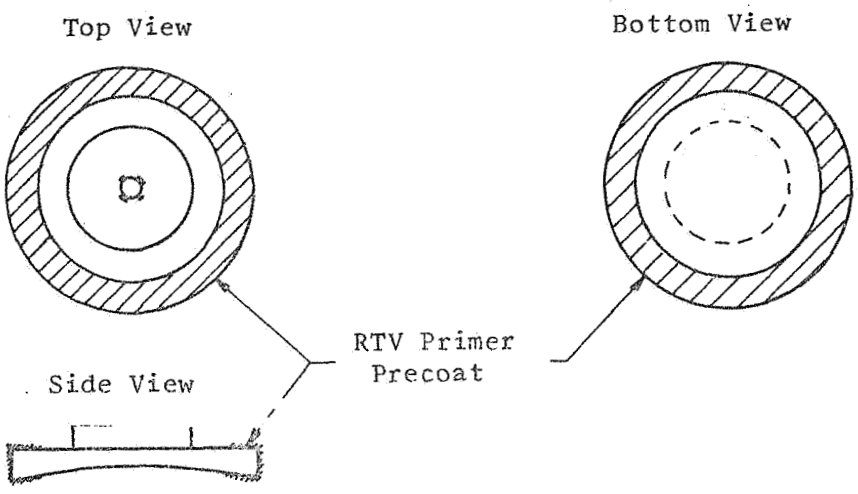

Figure 4. PRECOAT AREAS ON ATTACHMENT BLOCK AND SPECIMEN.

III, B, Recommended Sensor Attachment Procedures (cont.)

5. Apply a thin coat of light machine oil or a very thin coat of light silicone grease to the bottom surface of the mounting block (refer to Figure 5) and push the block securely into position with the silicone rubber precoated area on the specimen.

6. Keep the block in place and complete attachment by adding the RTV silicone rubber to produce a fillet around the attachment block which is smoothly feathered out to the specimen surface as shown in Figure 2. If the attachment block is applied to other than the top surface of a horizontal specimen, provide contact pressure to keep the block firmly in place and tight to the specimen surface while the RTV silicone rubber cures; 16 to 24 hr at room temperature is generally required. The mixture will become tack-free between 1 and 6 hr after mixing and the cure time can then be shortened by application of heat.

7. After the RTV silicone rubber has cured, but before mounting the sensor on the attachment block, either insert 3 or 4 drops of light machine oil in the threaded hole, or fill the hole approximately 1/2 to 3/4 full of light silicone grease. Also, apply a light coat of oil or a very light layer of grease directly to the base of the sensor; then thread the sensor into position and seat by applying the suggested torque (usually around 18 in.-lb).

8. Following testing, remove the attachment block using a sharp knife. Then carefully scrape or sand the residual rubber away. Removal can also be accomplished by use of a commercially available stripping solution (Ref 7), but care must be taken so as not to use a solvent which can produce corrosion or stress corrosion of the material being tested.

This sensor installation technique provides the degree of contact required for good stress-wave-emission transmissability through three

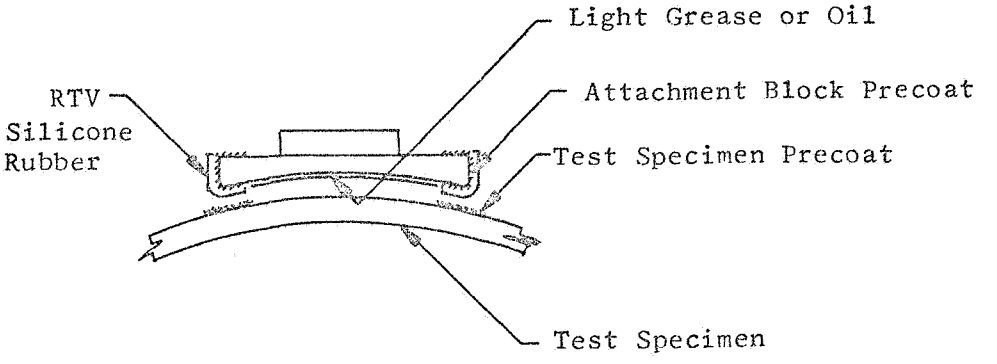

Figure 5. RTV SILICONE RUBBER PLACEMENT BEFORE POSITIONING OF THE ATTACHMENT BLOCK.

mechanisms: (1) a close fit between specimen surface and attachment block surface, (2) a light layer of oil or grease to provide a continuous film contact, and (3) the slight shrinkage of the cured RTV silicone rubber which securely positions the block to the specimen. No noises are experienced during specimen testing which originate from the attachment because the silicone rubber follows the elongation of the specimen identically and without cracking, while the attachment rides smoothly in place. The few drops of oil or light grease placed in the hole have been forced into the small volume between the block and the specimen, thus assuring an intimate and well-lubricated surface.

The room-temperature silicone rubber also resists and will withstand without degradation of physical or mechanical properties, all environmental conditions to which the SPS fuel tank is subjected. Its environmental limitations are near resistance as high as 600°F, low temperature flexibility to -65°F, and a brittle point of -95°F (Ref 7). The installation technique has been successfully used on the exterior surface of internally pressurized cylindrical titanium pressure vessels and on the exterior surfaces of externally pressurized glass spheres (20,000 psig external hydropressure) with excellent results.

In addition to the technique described above, other sensor attachment methods have been found acceptable. The main considerations are that they should not significantly attenuate the stress wave, should not be the source of stress-wave emissions due to cracking of adhesives or relative motion between the sensor and test specimen, and should provide good contact between the sensor and the test specimen. For example, successful sensor attachment to a pressure vessel has been obtained by the technique shown in Figure 6, where the sensor is held to the chamber by a wrap-around retaining cord. Figure 6 also shows a technique used in this program to mount sensors to the

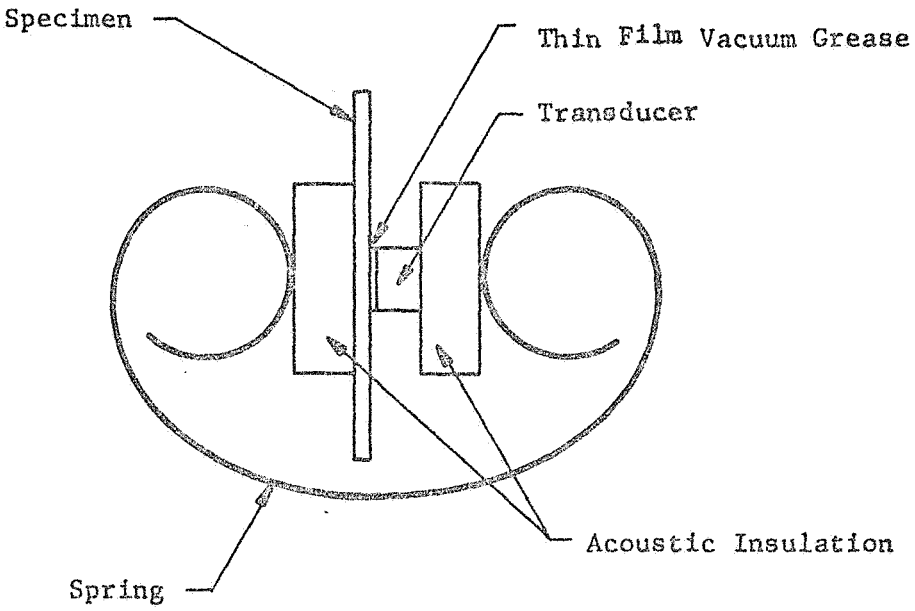

a. Specimen Attachment

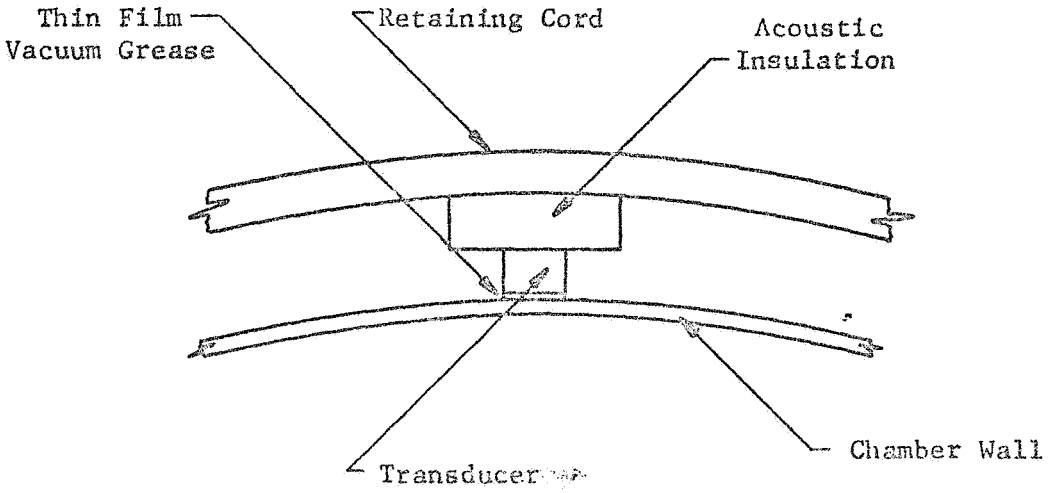

b. Chamber Attachment

Figure 6. Alternate Sensor Attachment Techniques

tensile test specimen during testing; the sensor being retained against the specimen by a wrap-around coiled spring. In both instances, a light film of vacuum grease or machine oil is used between the sensor and specimen. A cushion of acoustic foam is also placed between the retaining device and the sensor to reduce extraneous noise sources to a minimum. Although these procedures are acceptable sensor-mounting techniques and are less time consuming in comparison to the procedure previously described, they are more limited in application.

IV. STRESS-WAVE EMISSION CHARACTERISTICS

A. MATERIAL

The Ti-6Al-4V material used in this program was supplied by the NASA Manned Spacecraft Center, Houston, Texas, from a discarded service-propulsion-system propellant tank manufactured by Allison Division of General Motors. The material met the following chemical composition (wt %) requirements:

Al	V	Fe	H	C	N	O
5.5/6.75	3.5/4.5	0.30 max	0.0125 max	0.10 max	0.07 max	0.20 max

The total carbon plus nitrogen plus oxygen content also cannot exceed 0.30%.

The material had been heat treated by Allison as a 1/2-in.-thick forging by solution treating in the region of 50 to 60°F below the beta transus (approximately 1750°F), water quenching to room temperature, and aging at approximately 1000°F for 8 hours. Following fabricating, the 0.060-in.-thick tank was post-weld stress relieved at approximately 1000°F. Mechanical and metallurgical properties, as determined by Allison and NASA-MSC, indicated the microstructure to be equiaxed alpha-beta with a grain size of ASTM 5 or finer; the ultimate and yield strengths to be nominally 170 to 175 ksi and 160 to 165 ksi, respectively; and the plane strain fracture toughness (determined using 0.060-in.-thick PTC-tensile specimens) to be approximately 44 ksi-in.$^{1/2}$. The tank had seen approximately 250 service cycles without failure since its activation in 1965; this service included approximately 1000 hours of exposure to N_2O_4 and 4 hours of exposure to methl alcohol. The maximum stress during this service period was judged by NASA to be approximately 140 ksi. Nondestructive inspection by NASA of the test panels supplied for evaluation at Aerojet revealed neither pitting nor stress-corrosion cracking from the prior service history.

IV, Stress-Wave Emission Characteristics (cont.)

B. TEST PLAN

Two thicknesses (0.030 and 0.060-in.) were to be tested with three flaw shapes in each of three test media; viz., air, distilled water inhibited with sodium dichromate (500 ppm), and methyl alcohol. The part-through-crack (PTC) tensile specimen design used for these tests is shown in Figure 7. The 0.030-in.-thick material was obtained from the 0.060-in.-thick stock by machining material equally from both sides of the test specimen in the gage section. The 0.060-in.-thick specimens were tested in the as-received condition; the only surface preparation was a light sanding in the gage section.

Defects were initially introduced by electric-discharge machining (Eloxing) a tiny slot in the surface of each test piece using a chisel-shaped tungsten electrode. By varying the diameters of electrode (1/8, 1/16, and 1/32 in.), the size of the initial defect was varied. The Eloxed flaws were then sharpened by fatigue cycling each specimen in cantilever bending. This was accomplished using a electrodynamic shaker table. Table I lists the sample number, the corresponding "Elox" notch configuration and fatigue cracking data. After fatigue precracking, the specimens were to be tested in the following manner: (1) Load in a specified environment to a gross stress of 100 ksi for a minimum of 4 hr; (2) Fatigue cycle the test piece in air to outline any slow crack growth that may have occurred in step (1); (3) Reload to a gross stress of 125 ksi and hold for a minimum of 4 hr; (4) Again fatigue cycle to outline any slow crack growth that may have occurred in step (3); (5) Reload to a gross stress of 150 ksi and hold for a minimum of 4 hr; (6) Fatigue cycle to outline any slow crack growth that may have occurred in step (5); and finally, (7) Fracture the specimen in air by continuously increasing the load to failure.

In the first test (Sample No. 1, 0.060-in. thick), it was found that it was not possible to distinguish the various areas of slow crack growth by light

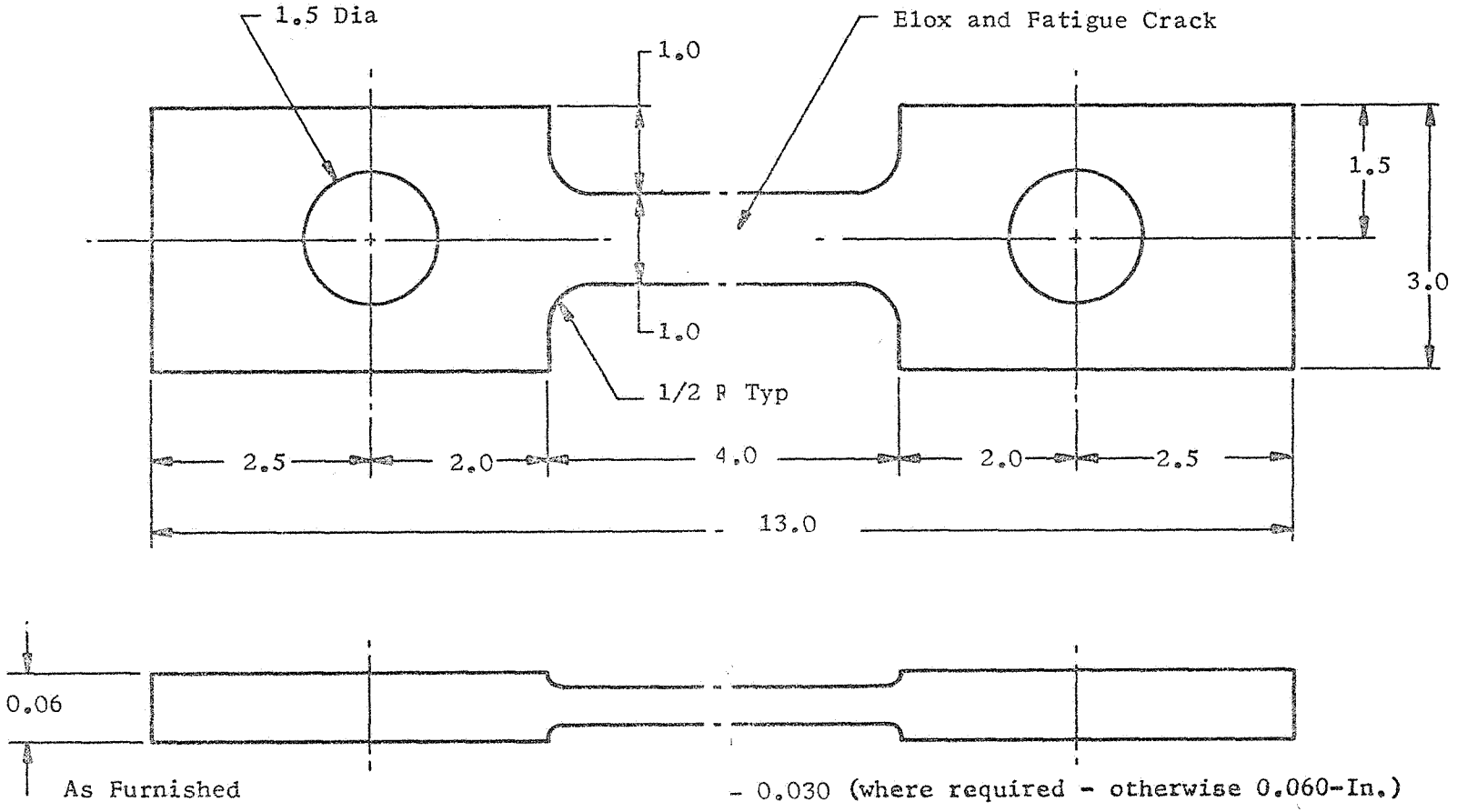

Figure 7. Part-Through-Crack Tensile Specimen.

TABLE I

FATIGUE PRECRACKING PARAMETERS

Sample No.	Elox Notch (a), in.	Crack Length (2c), in.	Fatigue Cycle		Fatigue Crack Dimensions	
			Load, ksi	Number of Cycles	Depth	Length
(0.030-IN.-THICK SPECIMENS)						
1	0.003	0.025[a]	NA[b]	NA	0.0298	0.350
2	0.003	0.026	NA	NA	0.024	0.156
			20.6	10,300	0.027	0.234
3	0.008	0.070	Two fatigue cracks			
4	0.003	0.027	NA	NA		
5	0.009	0.041	18.0	15,900	0.022	0.169
6	0.005	0.030	15.0	21,850		
			16.7	26,200		
			17.7	28,400		
			20.6	21,600	0.018	0.153
7	0.003	0.023[a]	NA	NA	0.028	0.266
8	0.005	0.039	21.0	21,000	0.019	0.192
9	0.003	0.022	17.7	19,440	0.022	0.173
(0.060-IN.-THICK SPECIMENS)						
1	0.021	0.098	33.4	17,300	0.025	0.110[c]
			[illegible]	[illegible]	[illegible]	[illegible]
2	0.019	0.084	48.7	5,400	0.031	0.132
			46.4	37,800	0.041	0.333
3	0.021	0.087	NA	NA	0.030	0.155
4	0.022	0.067	46.4	32,400	0.031	0.153
			33.4	27,750		
			35.4	25,000	0.038	0.222
5	0.021	0.047	51.6	21,600		
			30.9	14,100		
			33.4	74,800		
			35.4	17,500		
			33.4	43,200	0.036	0.156
6	0.022	0.051	46.4	27,900	0.034	0.109
7	0.021	0.083	35.4	26,600		
			33.4	27,750		
			35.4	80,000		
			33.4	34,400		
			30.9	20,000	0.031	0.139
8	0.026	0.080	30.9	24,400		
			28.4	167,500		
			36.0	149,000	0.037	0.138
9	0.023	0.051	36.0	175,000	0.030	0.091

(a) Burnt area caused by the Elox operation.

(b) Not Available. For the specimens fatigue cycled early in the program, it was difficult to obtain the number of cycles, the load was always less than 20 ksi for the 0.030-in.-thick specimens and less than 40 ksi for the 0.060-in.-thick specimens.

(c) Best estimate based on surface measurement.

microscopy; electron fractography had to be used to distinguish between the bands of environmental slow crack growth and fatigue cracking. The cost of electron fractography for this purpose would have been prohibitive. Also, since the specimens were to be fatigue cycled four times, the flaws would have tended toward the same shape and size, thus eliminating the initial difference in flaw shape.

The experience with the first test specimen dictated a major change in test procedure. Since the technique of fatigue cycling after environmental exposure was found to be impractical in the testing of such thin PTC-tensile specimens, it was necessary to change the procedure so that instead of loading each specimen to progressively higher stress (100 ksi, 125 ksi, and 150 ksi), each specimen was loaded to a specified stress intensity (K_I) value that was based on the estimated critical stress intensity factor. In a methyl alcohol environment, all test specimens failed within a relatively few hours regardless of the stress level used. However, in an air or inhibited water environment, with one anomaly, none of the test specimens failed; subsequent to prolonged periods of stress-environment exposure, these specimens were failed by raising the load to the critical stress intensity, K_{Ic}.

Table II lists specimen numbers, test environment, and corresponding load history. Figures 8 and 9 illustrate the fatigue crack and fracture faces for the 0.030 and 0.060-in.-thick specimens, respectively. It should be noted that two coplanar fatigue cracks developed in Specimens No. 3 and 6 (0.030-in. thick material).

C. FRACTURE MECHANICS CONSIDERATIONS

The part-through-crack tensile specimen incorporates a preflaw configuration which has been shown to have resulted in the service and hydro-test failures of numerous pressure vessels. Thus, with this specimen, it is

TABLE II

LOADING AND STRESS INTENSITY HISTORY

Sample No.	Thickness, in.	Width, in.	Crack Depth (a), in.	Crack Length (2c), in.	Load, lbs	Applied Stress Intensity, (K_I)	Test Time, min	Gross Stress, ksi	Test Environment
1	0.030	1.008	0.030[a]	0.350	2010	35.4	15	66.5	Methyl Alcohol
6	0.031	1.009	0.018	0.153[b]	2500	24.3	23	80.0	Methyl Alcohol
4	0.030	1.008		(a)= .474		No Good			
2	0.028	1.006	0.024	0.156	2940	44.4[d]	17,280	104.4	Water[c]
			0.027	0.234	2950	51.8[d]	Rising Load	104.8	Water
9	0.033	1.010	0.022	0.173	2500	26.6	3643	75.1	Water
			0.022	0.173	2900	31.4	265	87.0	Water
			0.022	0.173	3310	36.1[d]	1157	99.3	Water
			0.022	0.173	3560	38.9[d]	Rising Load	106.9	Water
8	0.033	1.012	0.019	0.192	2280	21.7	1088	68.3	Water
			0.019	0.192	2600	24.6	338	77.9	Water
			0.019	0.192	3220	30.6	263	96.4	Water
			0.019	0.192	3500	33.8	1135	104.8	Water
			0.019	0.192	3800	37.2	10	113.8	Water
3	0.032	1.010		20 = .278		Two Fatigue Cracks			Air
5	0.033	1.006	0.022	0.169	2600	27.9	988.5	78.3	Air
			0.022	0.169	3200	34.9	134	96.4	Air
			0.022	0.169	3700	40.6	290	111.3	Air
			0.022	0.169	3960	44.1[d]	Rising Load	119.2	Air
7	0.032	1.012	0.028	0.266	3000	45.5[d]	Rising Load	92.6	Air
9	0.061	1.005	0.030	0.091	6470	28.4	110	104.6	Methyl Alcohol
6	0.061	0.998	0.034	0.109	5300	27.2	166	87.1	Methyl Alcohol
3	0.062	1.008	0.030	0.155	5620	30.9	55	90.0	Methyl Alcohol

(a) The fatigue crack appears to have penetrated through the thickness.
(b) This specimen has two coplanar fatigue cracks.
(c) Distilled water plus 500 ppm sodium dichromate.
(d) K_{Ic} Value.

TABLE II (cont.)

Sample No.	Thickness, in.	Width, in.	Crack Depth (a), in.	Crack Length (2c), in.	Load, lbs	Applied Stress Intensity (K_I)	Test Time, min.	Gross Stress, ksi	Test Environment
2	0.062	1.012	0.031	0.132	5500	29.6	720	88.8	Water(c)
			0.041	0.333	5275	41.1(d)	Rising Load	83.1	Water
8	0.062	1.006	0.037	0.138	6830	42.6	91	109.6	Water
			0.037	0.138	7360	46.4	48	118.0	Water
			0.037	0.138	7900	50.1(d)	Rising Load	126.7	Water
5	0.062	0.995	0.036	0.156	4850	29.3	209	78.6	Water
			0.036	0.156	6200	39.0	3990	100.4	Water
			0.036	0.156	7870	47.1(d)	Rising Load	119.5	Water
1	0.061	1.002	0.025	0.110	5580	27.2	270	91.5	Air
			0.025	0.110	5575	27.2	172	91.5	Air
			0.025	0.110	5575	27.2	220	91.5	Air
4	0.062	0.990	0.031	0.153	4300	24.4	540	70.0	Air
			0.031	0.153	5410	30.9	996	88.2	Air
			0.038	0.222	5300	37.1	4326	86.3	Air
			0.038	0.222	5885	41.4(d)	Rising Load	95.8	Air
7	0.062	1.013	0.031	0.139	6040	33.1	1075	96.1	Air
			0.031	0.139	6700	37.0	357	106.7	Air
			0.031	0.139	7250	40.1	1162	115.3	Air
			0.031	0.139	7700	42.9	140	122.6	Air
			0.031	0.139	8350	47.1	1066	133.0	Air
			0.031	0.139	8850	50.1(d)	Rising Load	141.0	Air

(c)Distilled water plus 500 ppm sodium dichromate
(d)K_{Ic} Value.

Sample No.

Tested in Methyl Alcohol

1

4

6

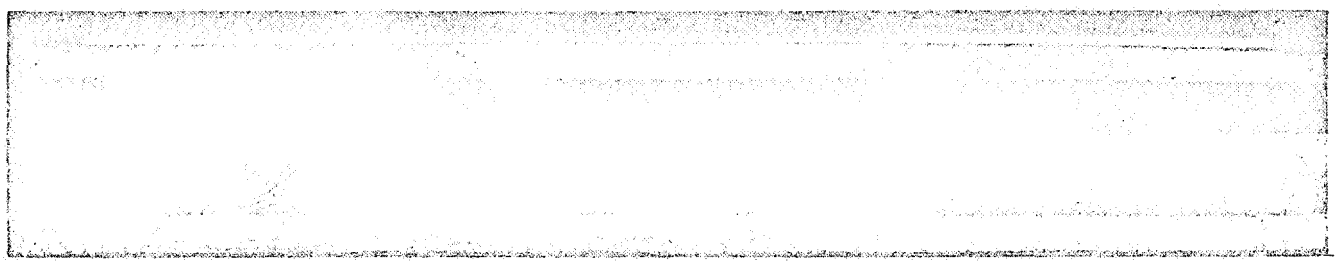

Tested in Distilled Water Plus 500 PPM Sodium Dichromate

9

8

2

Tested in Air

3

5

7

Figure 8. Fracture Faces of 0.030-in.-Thick 6Al-4V Titanium Alloy

Sample No.

Tested in Air

1

4

7

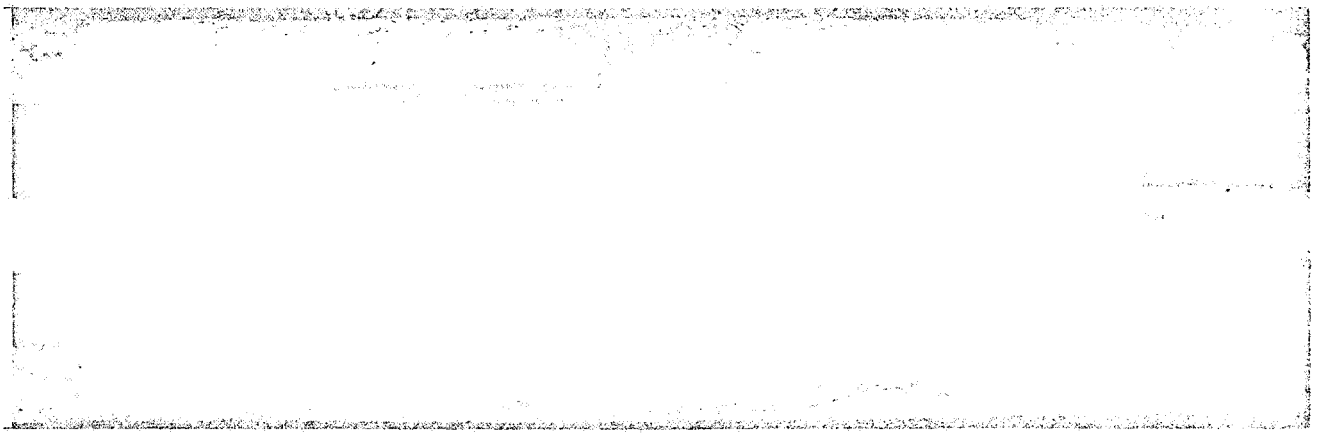

Tested in Distilled Water plus 500 PPM Sodium Dichromate

2

5

8

Tested in Methyl Alcohol

3

6

9

Figure 9. Fracture Faces of 0.060-in.-Thick 6Al-4V Titanium Alloy

possible to duplicate in the laboratory, stress-flaw-environment conditions which are frequently encountered in service failures. The following relationship was derived by Irwin (Ref 8) for calculation of stress intensity values in part-through-crack tensile testing:

$$K_{Ic}^2 = \frac{1.21 \pi a F^2}{Q}$$

$$K_{Ic} = 1.95 F (a/Q)^{1/2} \qquad \text{(Eq 1)}$$

where a is the crack depth, F is the gross stress, and Q is a flaw-shape parameter (see Figure 10).

The stress-intensity solution for a semi-elliptical surface flaw as derived by Irwin has been found to be reasonably accurate for flaw depths up to approximately 50% of the material thickness. At greater depths, the applied stress intensity is magnified because of the effect of the free surface near the flaw tip. This means that in thin-walled vessels (i.e., vessels where the critical flaw size approaches or exceeds the wall thickness), the flaw-tip stress intensity can attain the critical K_{Ic} value at a flaw size which is significantly smaller than that which would be predicted using the equation as derived by Irwin. Kobayashi (Ref 9) has developed a solution for deep surface flaws which are long with respect to their depth ($a/2c < 0.30$), and Smith (Ref 10) has developed a solution for semicircular surface flaws (i.e., $a/2c = 0.5$). The results are shown in Figure 11 in terms of a stress intensity magnification factor, M_k, plotted against the crack-depth-to-thickness (a/B) ratio. This factor is applied to the original Irwin equation to obtain the stress intensity for deep surface flaws. It is seen that the magnification factor reaches a minimum value of less than 10% for semicircular flaws, whereas an increase of about 60% is observed for flaws with small a/2c values.

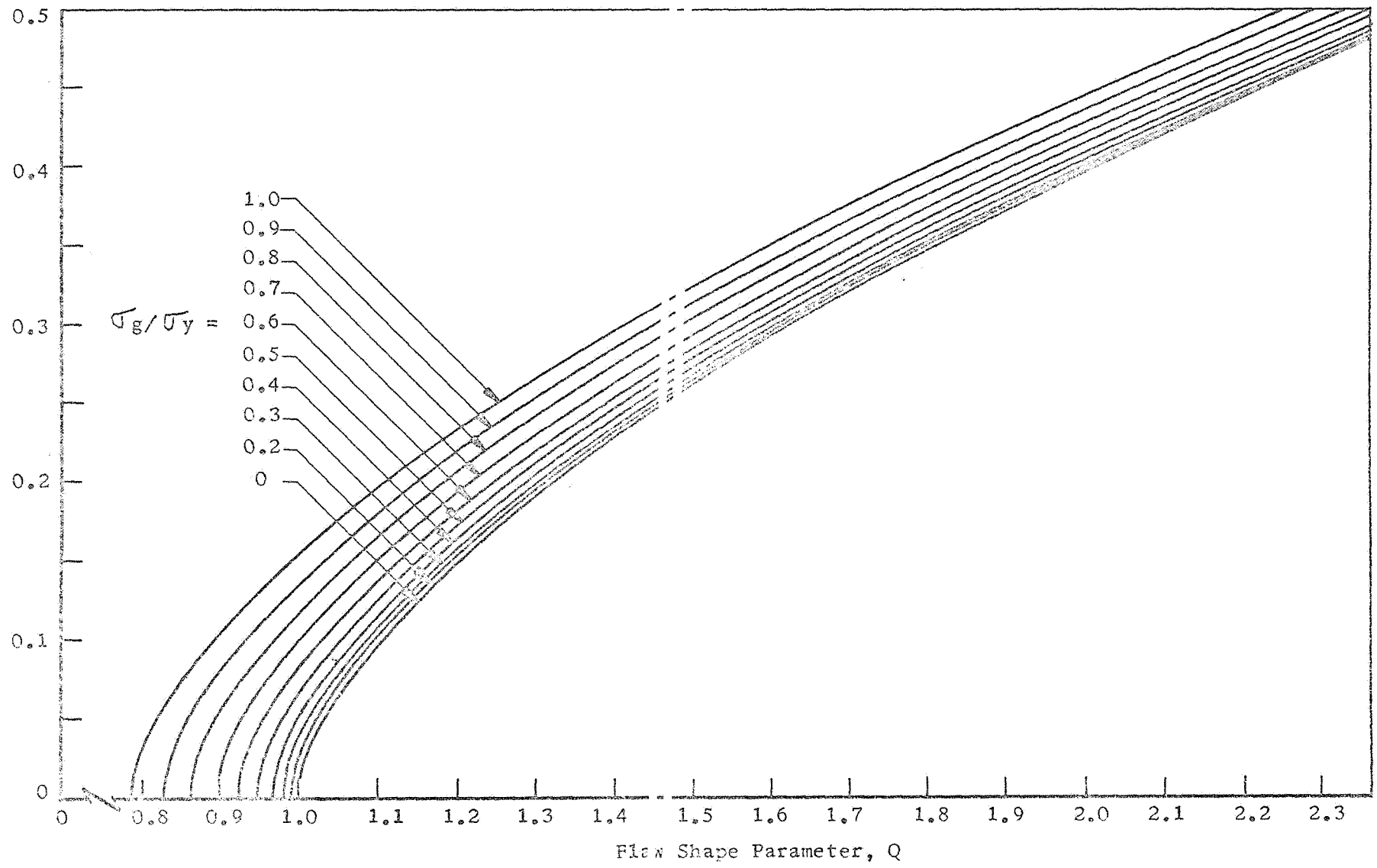

Figure 10. Shape Parameter Curves for Surface and Internal Flaws.

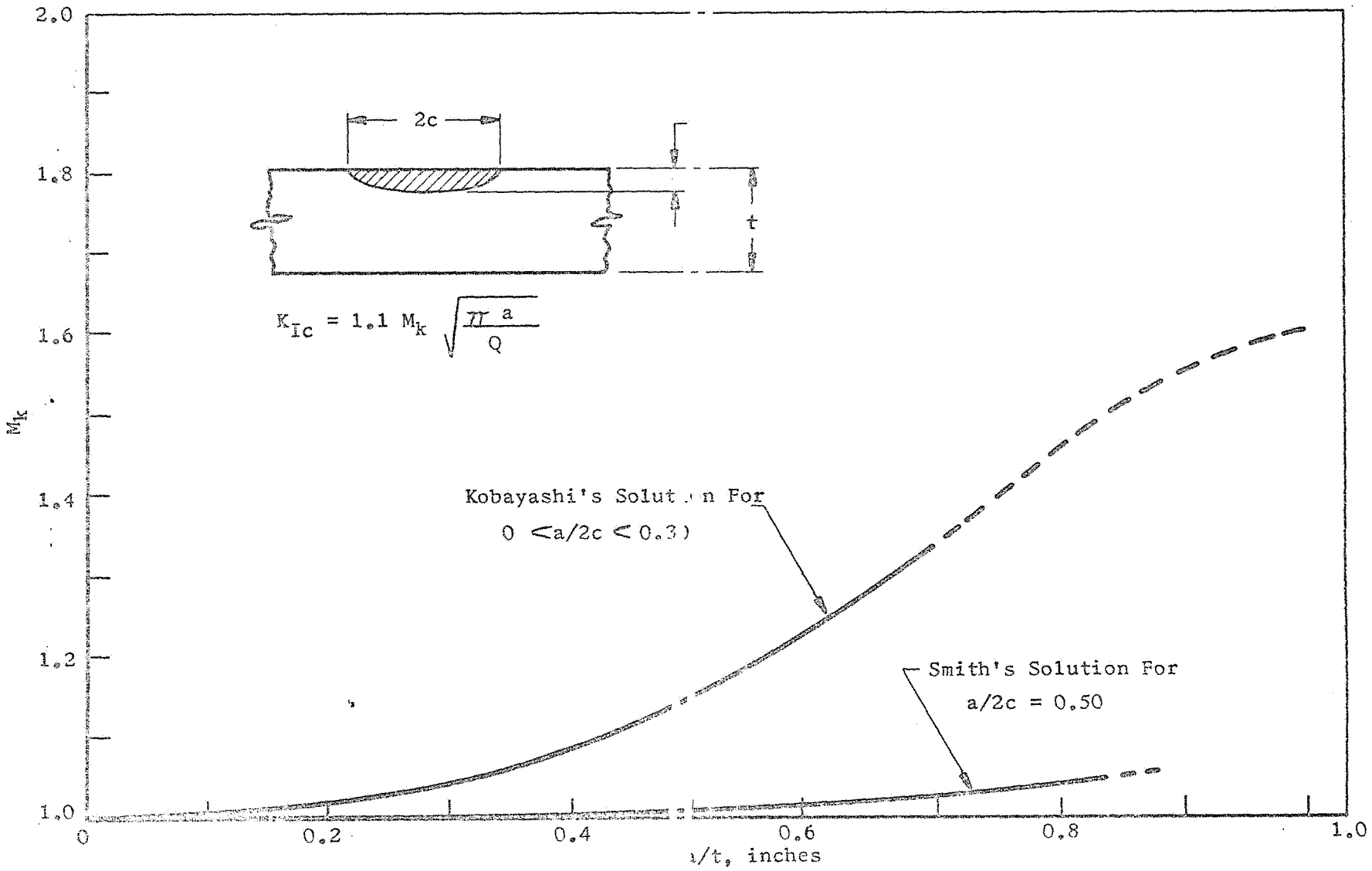

Figure 11. Stress Intensity Magnification Factors for Deep Surface Flaws

D. STRESS-WAVE EMISSION INSTRUMENTATION AND DATA ANALYSIS

The instrumentation used to acquire stress-wave emission data in this program is shown schematically in Figure 12 and consists of accelerometers, amplifiers, filters, tape recorders, a frequency switch and an electronic counter and digital printer. The accelerometers were attached to the specimens using the linear force-coiled spring technique shown in Figure 6.

As indicated in Figure 12, two basic systems were employed for stress-wave emission data acquisition. The electronic counter system was employed for all tests and provided a real-time automatic count of the stress-wave emission rate throughout each test period. Typical stress-wave-emission data from the counter-printer is shown in Table III.

The high-pass filter used in the system eliminates a major portion of the extraneous low-frequency noises which tend to mask very small amplitude stress waves. In a similar manner, the frequency switch is a signal discriminating circuit developed at Aerojet, which eliminates much of the spurious instrumentation-noise signals which do not contain the characteristics of stress waves. This switch basically looks at the amplitude and frequency content of a signal and provides a pulse output for each stress wave and no output for noise signals. The pulse output is provided as an input to the electronic counter(s), which then collect and tabulate total count and rate of stress-wave-emission data.

The second data acquisition system was employed during the testing of selected specimens exposed to each of the test environments. This acquisition system also used the amplification and filtering components but incorporated a magnetic tape recorder. The magnetic tape recordings were made either by direct recording or by rerecording from a tape-loop recorder.

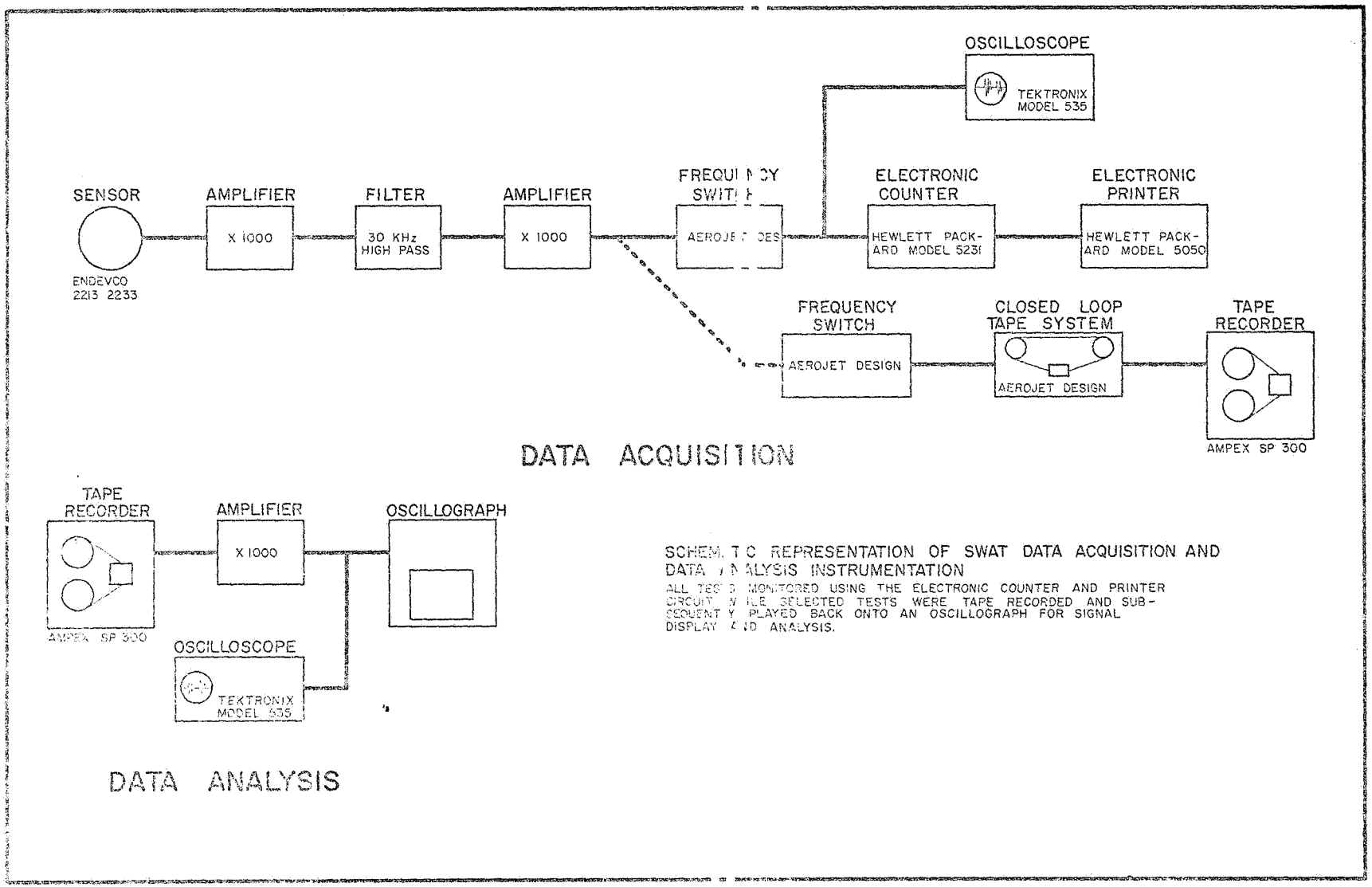

Figure 12. Schematic Representation of SWAT Data Acquisition and Data Analysis Instrumentation

TABLE III

COUNTER DATA FROM PRINTER
SAMPLE NO. 1, 0.030-IN.-THICK, TESTED IN METHYL ALCOHOL
Ti-6Al-4V ALLOY

Ten Second Interval	SWE Per Ten Seconds	Average SWE per Second	Minute Intervals	SWE Per Minute	Average SWE Per Second
1	4	0.4			
2	5	0.5			
3	1	0.1			
4	3	0.3			
5	2	0.2			
6	0	0	1	15	0.25
7	0	0			
8	0	0			
9	0	0			
10	2	0.2			
11	0	0			
12	0	0	2	2	0.03
13	0	0			
14	0	0			
15	0	0			
16	0	0			
17	0	0			
18	0	0	3	0	0
[illegible]	0	0			
20	0	0			
21	1	0.1			
22	1	0.1			
23	0	0			
24	0	0	4	2	0.03
25	0	0			
26	2	0.2			
27	0	0			
28	0	0			
29	0	0			
30	0	0	5	2	0.03
31	0	0			
32	1	0.1			
33	1	0.1			
34	0	0			
35	0	0			
36	0	0	6	2	0.03
37	2	0.2			
38	1	0.1			
39	0	0			
40	0	0			
41	0	0			
42	0	0	7	3	0.05
43	0	0			
44	0	0			
45	0	0			
46	0	0			
47	0	0			

TABLE III (cont.)

Ten Second Interval	SWE Per Ten Seconds	Average SWE per Second	Minute Intervals	SWE Per Minute	Average SWE Per Second
48	0	0	7	3	0.05
49	0	0			
50	0	0			
51	0	0			
52	0	0			
53	0	0			
54	0	0	9	0	0
55	0	0			
56	0	0			
57	3	0.3			
58	0	0			
59	0	0			
60	0	0	10	3	0.05
61	0	0			
62	0	0			
63	0	0			
64	2	0.2			
65	2	0.2			
66	0	0	11	4	0.07
67	0	0			
68	0	0			
69	0	0			
70	0	0			
71	1	0.1			
72	0	0	12	1	0.02
73	1	0.1			
74	0	0			
75	0	0			
76	1	0.1			
77	1	0.1			
78	0	0	13	3	0.05
79	0	0			
80	1	0.1			
81	1	0.1			
82	1	0.1			
83	28	2.8			
84	13	1.3	14	44	0.73
85	12	1.2			
86	10	1.0			
87	13	1.3			
88	47	4.7 (Failure)			

During longtime tests, the cost of tape and the possibility of running a test beyond the time represented by a single reel of tape requires that the closed-loop system of data acquisition be used. This system consists of a loop-to-recorder reproducer and a remote-controlled tape recorder. The loop recorder is run continuously and transfers the stress-wave data recorded on the loop to the remote-controlled tape recorder whenever a signal is recorded above a selected amplitude. In this manner, long-time tests can be compressed onto tape recordings of a reasonable length. Periods in which no stress-wave emission data occurs are not transferred to the remotely controlled recorder. Shorter-term tests or tests under constantly changing conditions, such as during rising load periods, are usually recorded directly on magnetic tape without use of the tape-loop recorder. All taped data are then played back and recorded, for analysis, through a light-beam galvanometer oscillographic recorder onto photographic paper; a typical oscillogram is shown in Figure 13.

The sinusoidal frequency response of the record-playback system is maintained as high as possible to preserve the fidelity of the original signal. It should be noted, however, that the stress-wave emission itself is a transient wave of a pulse nature and its recorded quality may bear little relationship to a system whose frequency response is determined by a periodic function.

E. DISCUSSION OF RESULTS

1. Critical Stress Intensity

The critical stress intensity (K_{Ic}) values obtained for the 0.030 and 0.060-in.-thick materials are shown in Table II and averaged 43.5 ksi-in.$^{1/2}$ and 45.9 ksi-in.$^{1/2}$, respectively. These values agree well with the value of 44 ksi-in.$^{1/2}$ obtained by NASA for the 0.060-in.-thick material

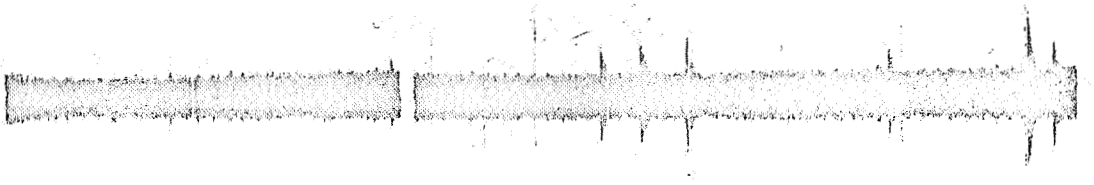

68 sec Prior to Failure

133 ksi Gross Stress

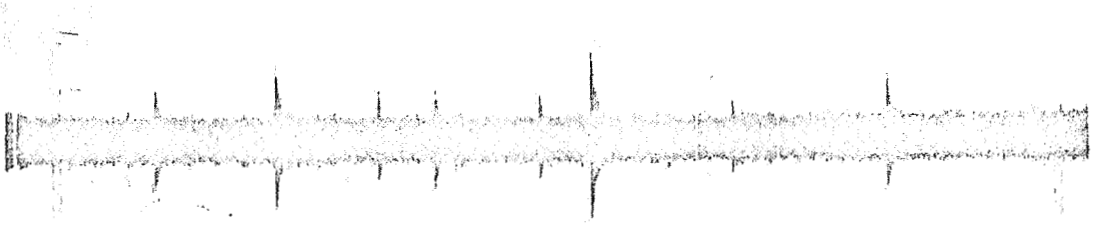

43 sec Prior to Failure

Failure
141 ksi Gross Stress

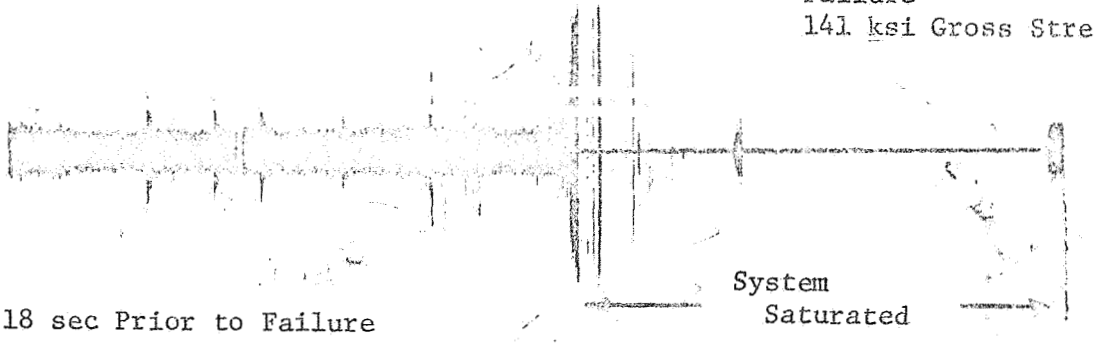

18 sec Prior to Failure

Figure 13. Oscillogram of Specimen No. 7 (0.060-in.-Thick) 6Al-4V Titanium Alloy Tested in Air, Failed in Rising Load

used in this program. From Table II, it is also apparent that there was no significant difference in the K_{Ic} value as a function of testing in either an air or inhibited water environment. This would be expected, since previous studies (Ref 11) have shown that while environment may vary the rate of slow-crack growth, it does not alter the critical combination of stress and crack size required for failure. Since the measurement of environmentally induced flaw extension in methyl alcohol would have required electron fractography, critical stress intensity values were not calculated for tests in this environment.

The apparent stress-intensity values of 43.5 and 45.9 ksi-in.$^{1/2}$ for the 0.030 and 0.060-in.-thick material may not be valid K_{Ic} values according to a criterion set down by Brown and Srawley (Ref 12); their criterion specifies that the specimen thickness must equal or exceed 2.5 $(K_{Ic}/F_{ty})^2$ for a valid K_{Ic} determination. For a K_{Ic} of 44 ksi-in.$^{1/2}$ and a yield strength of 160 ksi, the minimum thickness would be 0.19-in.; thus, where the thickness of material available for test is only 0.060-in., it is not possible to obtain a valid K_{Ic} value according to this criterion. However, in a recent study of 6Al-4V titanium as used in the 52-in.-dia second-stage Minuteman rocket motor case (Ref 13), it was observed that the 2.5 $(K_{Ic}/F_{ty})^2$ criterion is too restrictive in PTC-tensile test measurements of K_{Ic}. Likewise, the criterion has been shown to be overly conservative in PTC-tensile tests of grade-200 18% nickel maraging steel (Ref 14). From the Minuteman data-collection program (Ref 13), when the data from 0.125-in.-thick, shallow-cracked, PTC-tensile specimens were plotted on probability paper (several hundred tests), the population mean value of K_{Ic} was 39.1 ksi-in.$^{1/2}$, with a standard deviation of 1.6 ksi-in.$^{1/2}$.

IV, E, Discussion of Results (cont.)

2. Effect of Applied Stress Intensity (K_{Ii})

The applied stress intensity data in Table II and plotted in Figure 14, illustrate the pronounced effect of environment on stress corrosion cracking of the Ti-6Al-4V alloy. When tested in an air or inhibited water environment (except for Specimen 8, 0.03-in.-thick), neither slow-crack growth nor failure was observed during hold periods of up to 18 hours at applied stress intensity values of up to 92% of K_{Ic} (0.92 K_{Ic}). In methyl alcohol, on the other hand, the time to failure was found to be dependent upon the applied stress intensity level. Note, also, that in the semi-log plot of Figure 14, it was possible to draw a straight line through all but one data point; moreover, the straight line extrapolated to $K_{Ii}/K_{Ic} = 1$. The one data point off the straight line was from Specimen No. 6, which involved two coplanar fatigue cracks approximately 0.2-in. apart*.

3. Stress-Wave-Emission Characterization

a. Laboratory evaluations

Typical plots of stress-wave count rate (SWE/time) for the various materials and environments investigated are shown in Figures 15 through 21. The stress-wave data were consistent with the fact that in air and inhibited water, with one exception**, the test specimens did not fail

*Because of the straight line, it is possible to estimate the effect of the two coplanar fatigue cracks on specimen failure. For failure to occur in 26 minutes, as it did in Specimen No. 6, the applied stress intensity factor would be approximately 0.7 K_{Ic} with a single surface flaw. However, in Specimen No. 6, the stress intensity level was calculated to be approximately 0.5 K_{Ic} assuming a single surface flaw is produced at the eloxed defect. Thus, it appears that the effective flaw was larger than that used in the calculation; i.e., there must have been an interaction of the two coplanar flaws.

**Specimen No. 8, after a succession of holds at increasingly higher stress intensity levels, failed after only 10 minutes at an applied stress intensity level of 37.2 ksi-in.$^{1/2}$. No explanation was found for this one anomalous test.

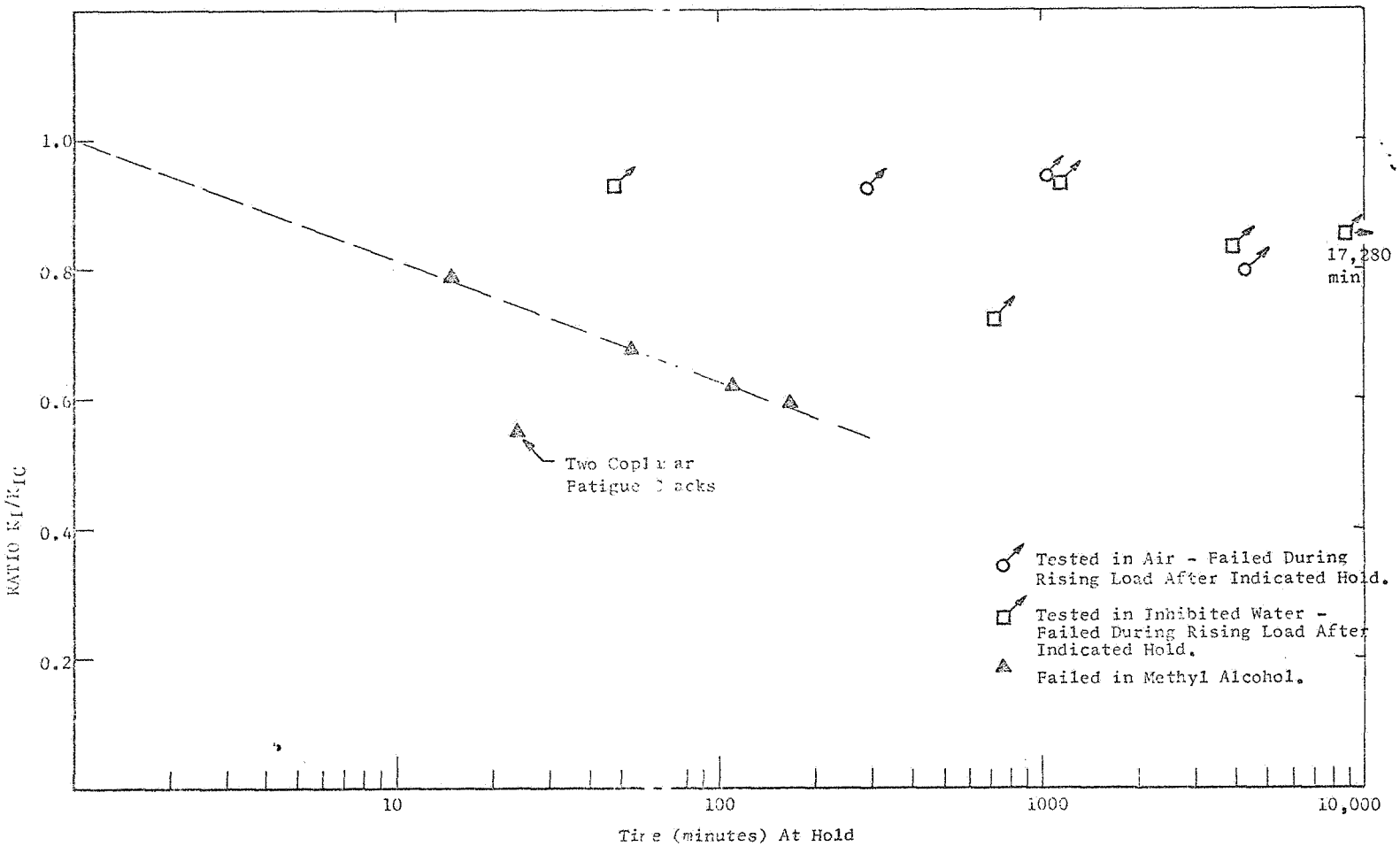

Figure 14. Applied Stress Intensity vs Time at Hold, (Part-Through-Crack Titanium 6Al-4V in Air, Inhibited Water, and Methyl Alcohol)

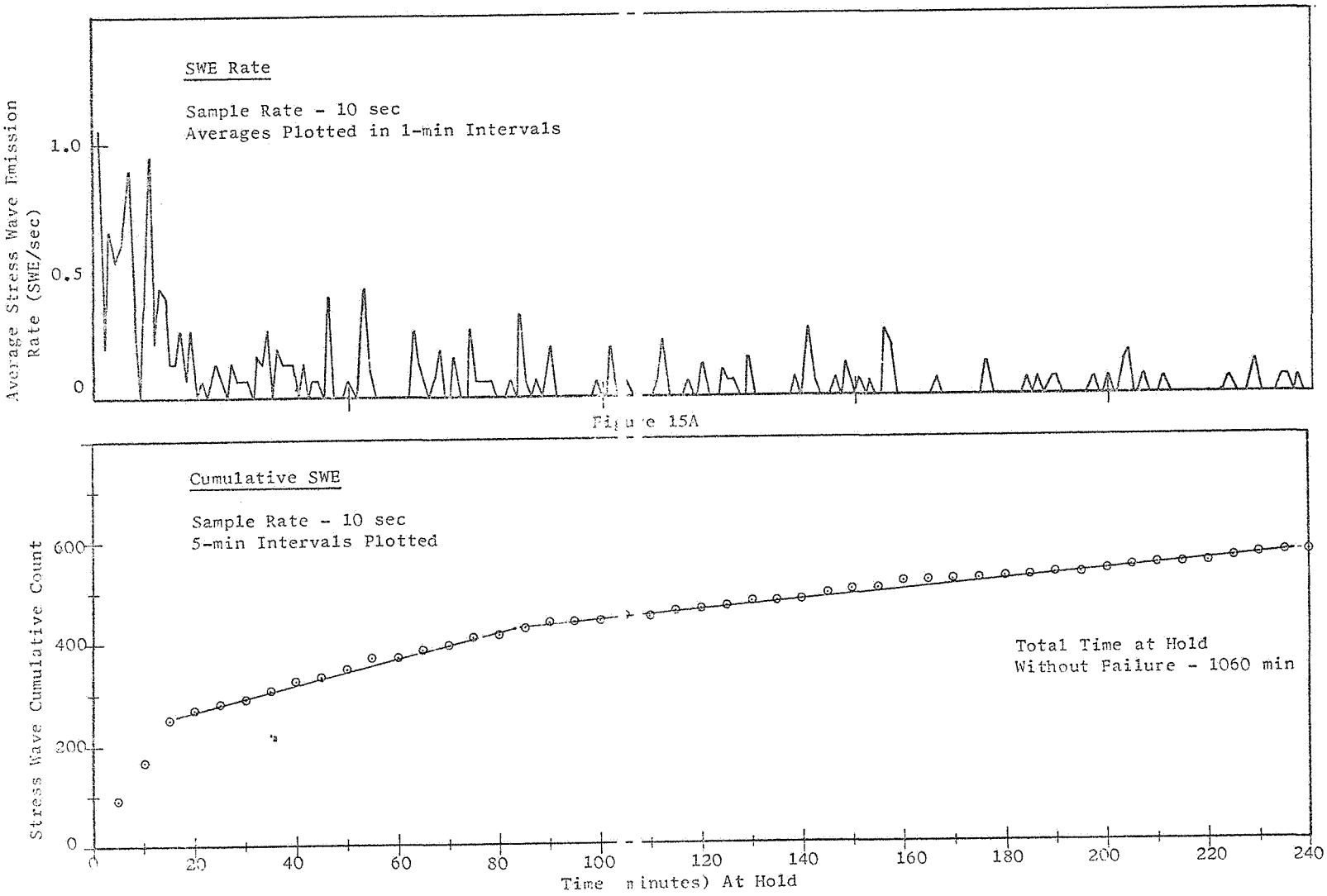

Figure 15. Stress Wave Emission Data vs Time at Hold (Specimen No. 7, 6Al-4V Titanium, 0.060-in.-Thick, $K_{Ii} = 0.94\ K_{Ic}$, Tested in Air)

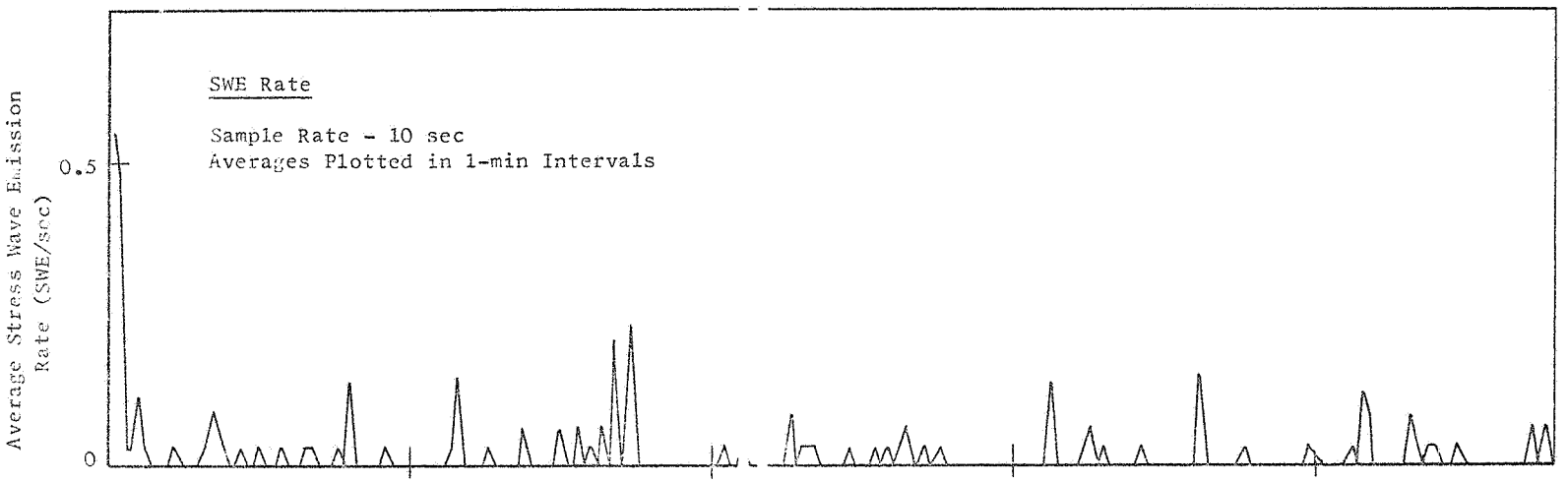

FIGURE 16A

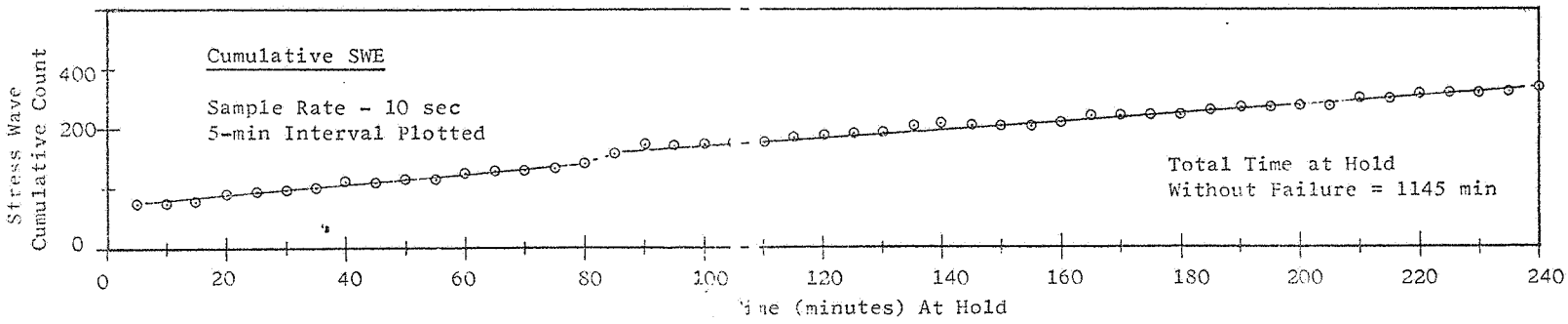

Figure 16. Stress Wave Emission Data vs Time at Hold (Specimen No. 9, 6Al-4V Titanium, 0.030-in.-Thick, $K_{Ii} = 0.93\ K_{Ic}$, Inhibited Water)

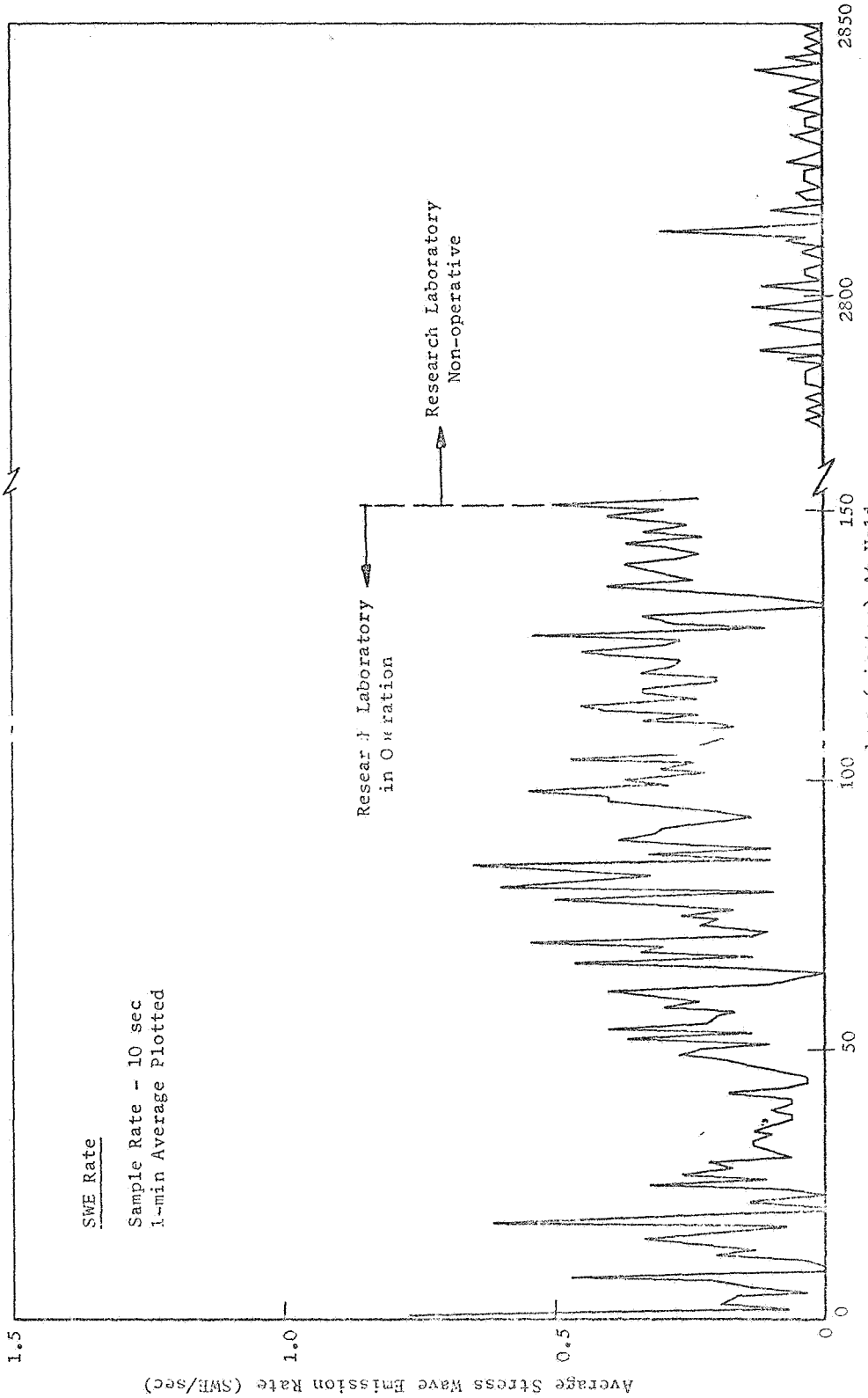

Figure 17. Stress Wave Emission Data vs Time at Hold (Specimen No. 5, 6Al-4V Titanium 0.060-in.-Thick, K_{Ii} = 0.83 K_{Ic}, Tested in Inhibited Water)

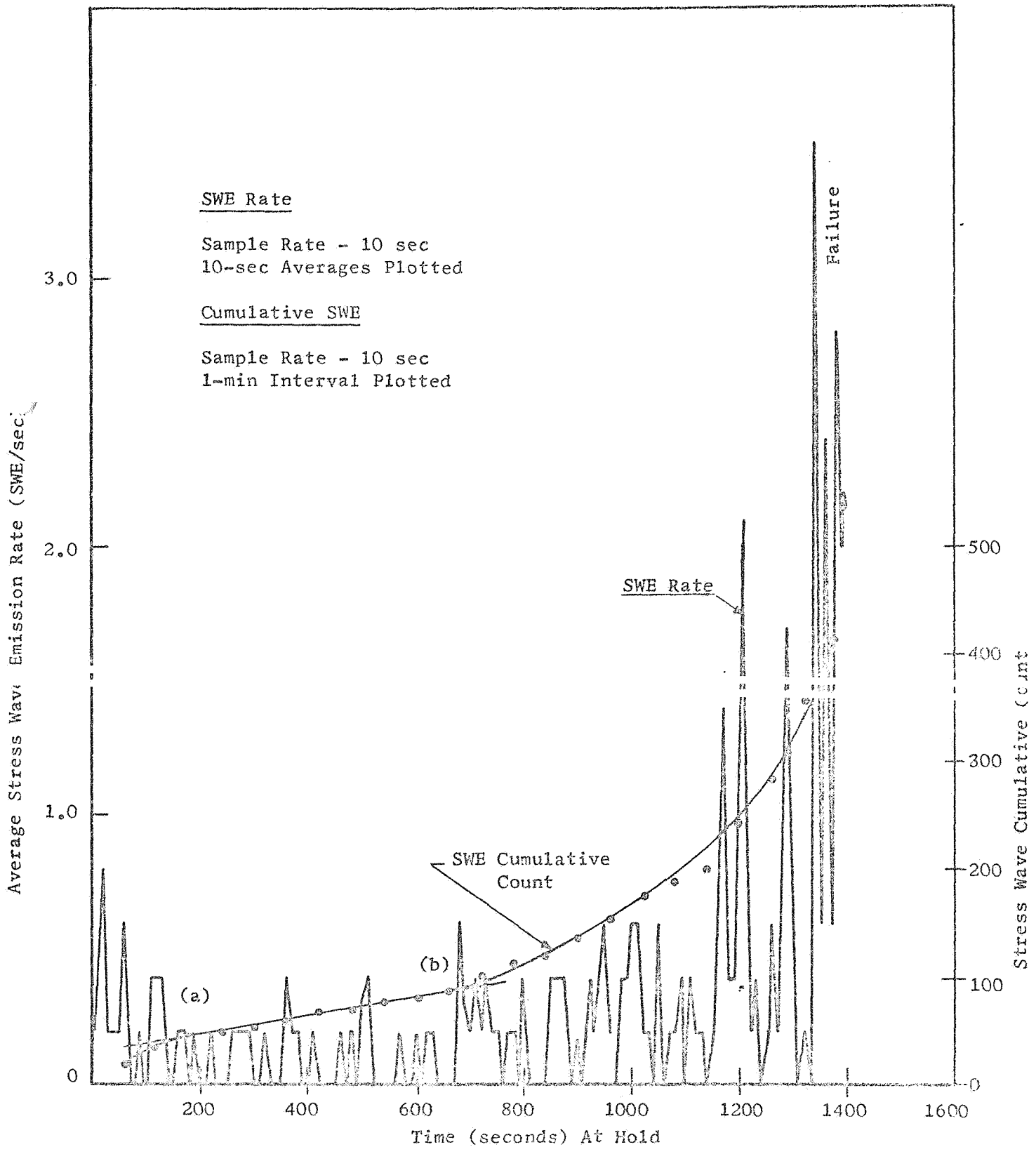

FIGURE 18

STRESS WAVE EMISSION DATA vs TIME AT HOLD (Specimen No. 6, 6Al-4V Titanium, 0.030-in.-thick, $K_{Ii} = 0.56\ K_{Ic}$, Tested in Methyl Alcohol)

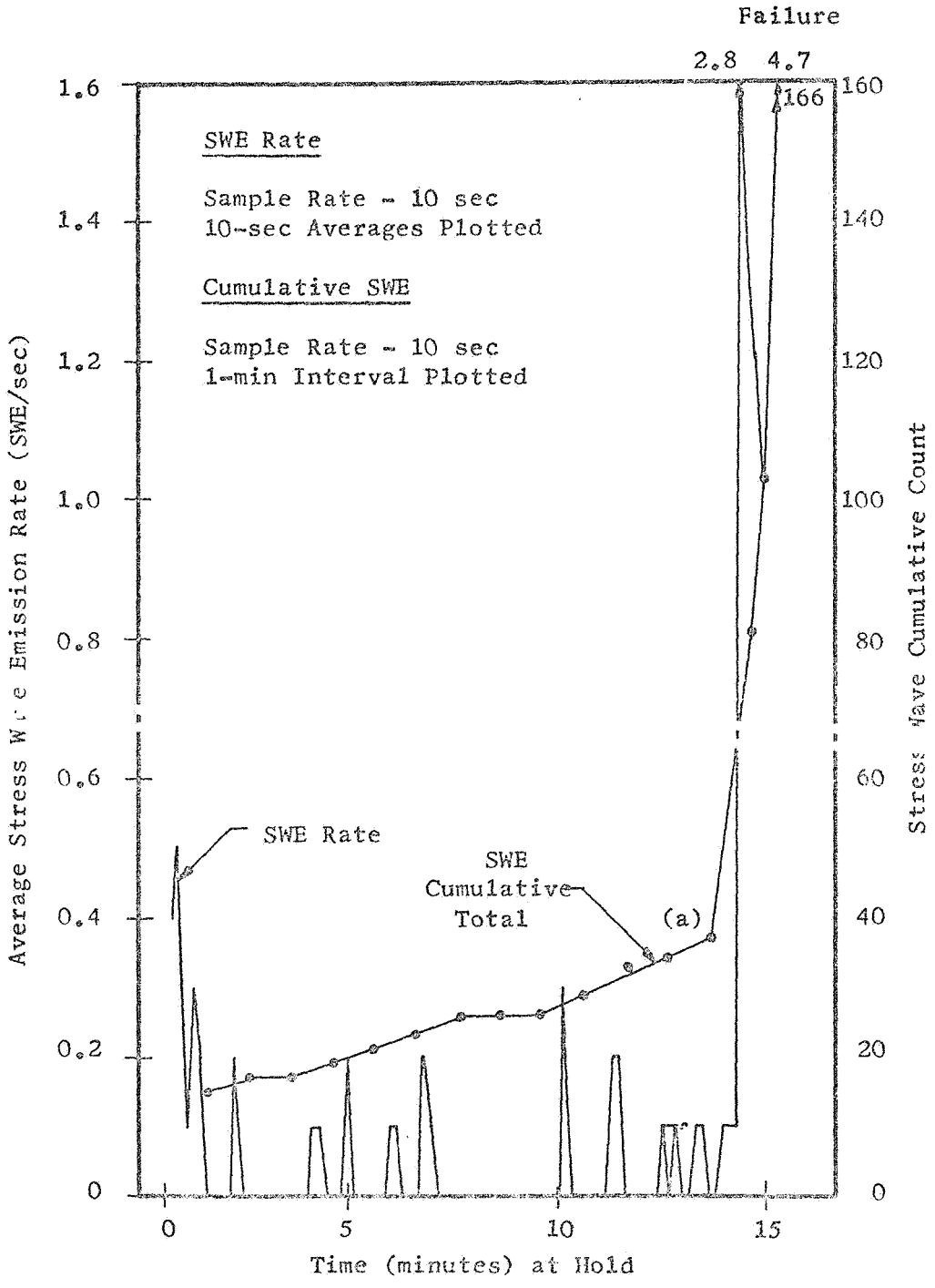

FIGURE 19

STRESS WAVE EMISSION DATA vs TIME AT HOLD (Specimen No. 1, 6Al-4V Titanium, 0.030-in. Thick, $K_{Ii} = 0.81\ K_{Ic}$ Test in Methyl Alcohol)

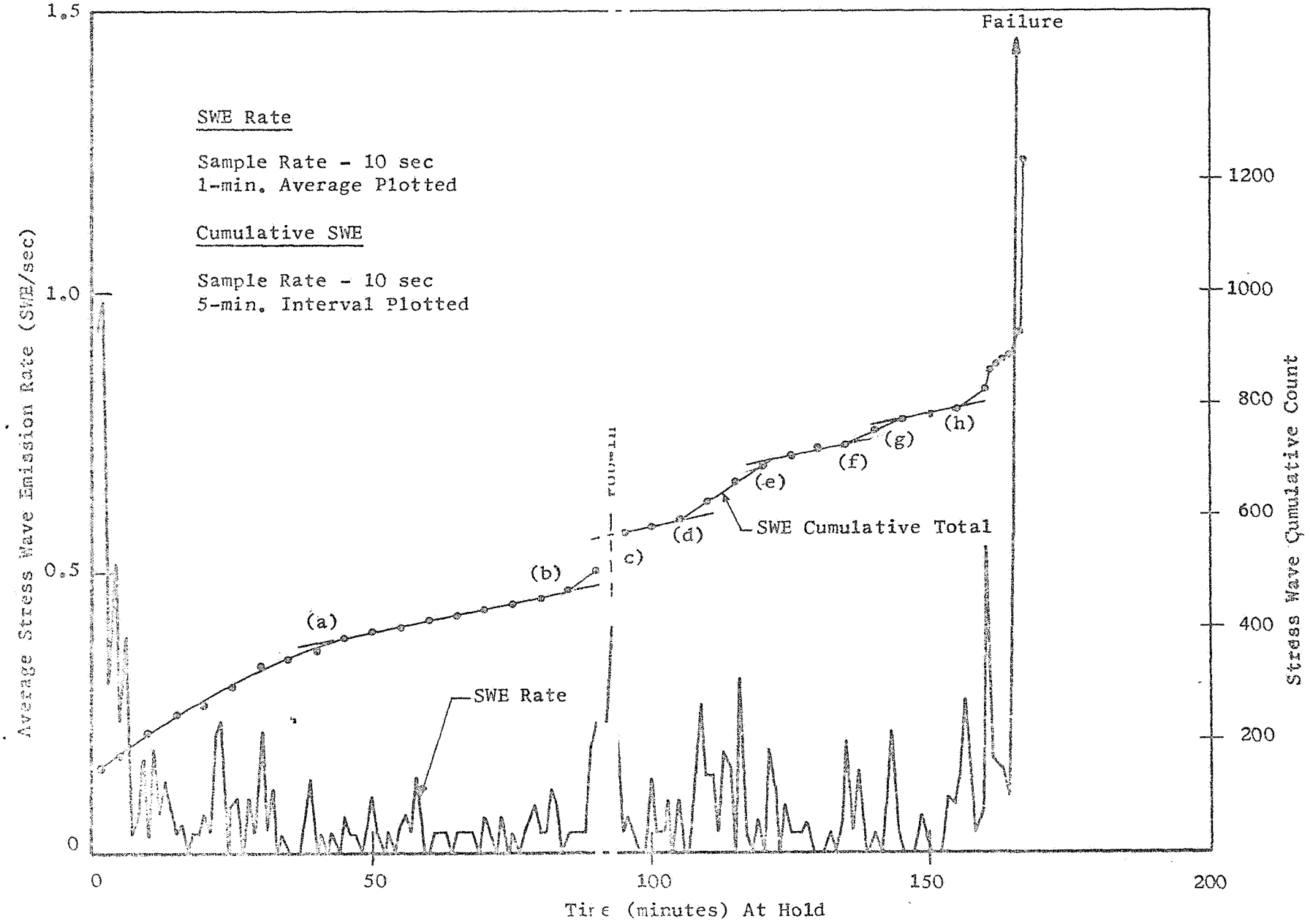

FIGURE 20

STRESS WAVE EMISSION DATA vs TIME AT HOLD
(Specimen No. 6, 6Al-4V Titanium, 0.060-in.-thick, $K_{Ii} = 0.59\ K_{Ic}$, Tested in Methyl Alcohol)

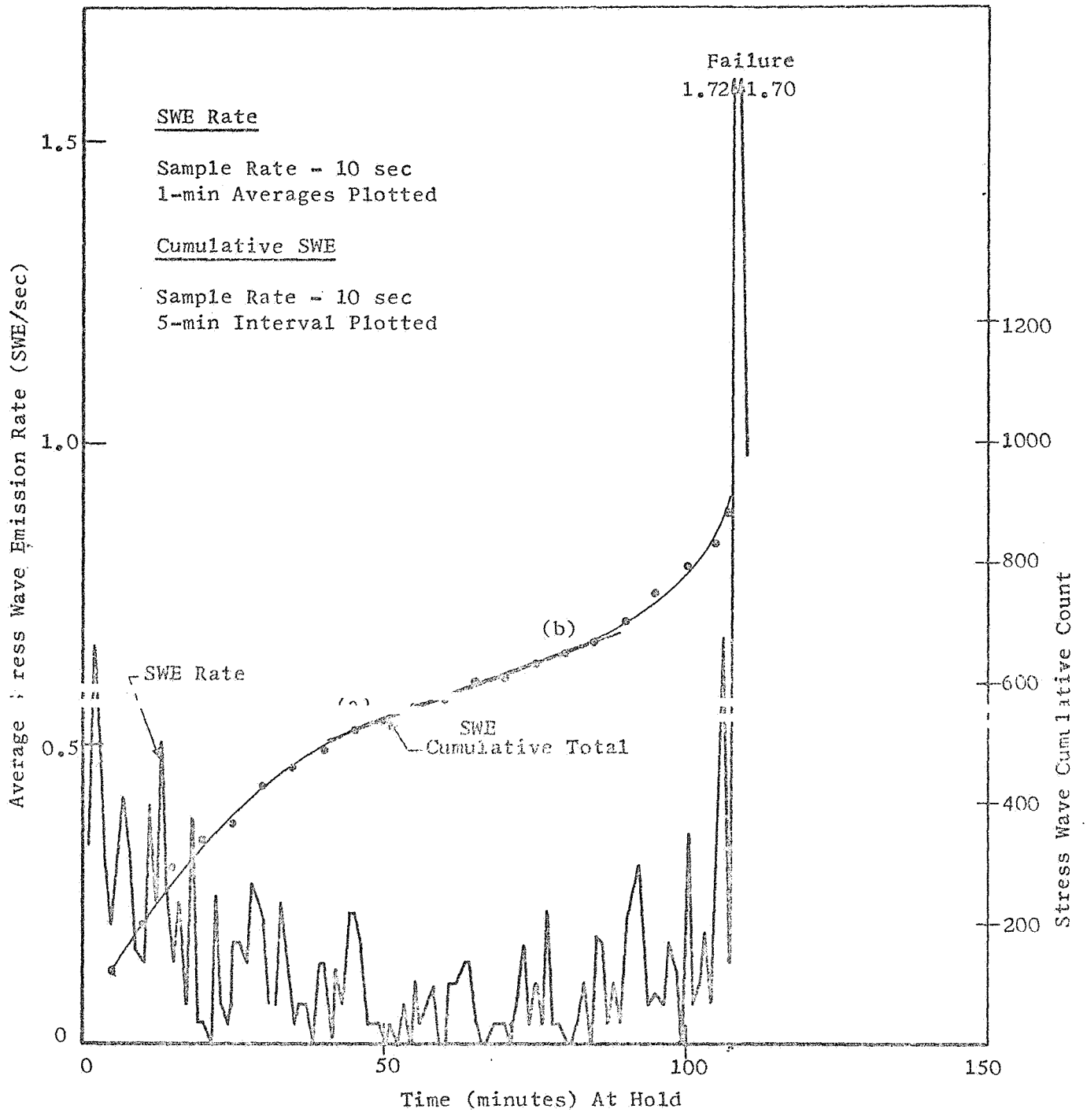

FIGURE 21

STRESS WAVE EMISSION DATA vs TIME AT HOLD (Specimen No. 9, 6Al-4V Titanium, 0.060-in. Thick, $K_{Ii} = 0.62\ K_{Ic}$, Tested in Methyl Alcohol)

under sustained load for long periods of time. In these environments, the plots of stress-wave count rate showed no evidence of crack growth; whereas, in methyl alcohol, the stress-wave data produced strong evidence of crack growth.

In Figures 15 through 21, the data are presented in two ways; one is a plot of stress-wave count rate (SWE/time) versus time at hold, and the other is the cumulative number of stress waves versus time at hold. Both types of data presentation provide a basis for terminating a test prior to failure. The plot of SWE/time versus time at hold is useful in determining the critical SWE rate preceiding failure. The plot of cumulative SWE versus time at hold provides a means for distinguishing crack growth from background noise and detecting the onset of instability. If the cumulative SWE plot has a constant slope, the detected signals can be attributed to background noise; whereas, if the slope is increasing, crack growth is occurring (see Figure 18). As crack growth continues, the slope of the line will increase exponentially, until it is nearly vertical at failure. In addition, in practice where a real time data printout SWAT system, including triangulation back to the source of the emission, would be employed, the random nature of background noise would be easily distinguishable from the single source of emissions associated with the growth of a flaw. Observation of the data on an oscilloscope during a test would also distinguish crack induced stress waves from noise.

The data in Figures 18 through 21 indicate a comparatively large number of stress waves is sometimes observed at the start of hold which gradually decreased in number with time; this is thought to be due to initial crack tip adjustment resulting in blunting of the crack and has been observed in most of the laboratory tests conducted at Aerojet where SWE have been employed to monitor fracture in structural metals.

IV, E, Discussion of Results (cont.)

The SWE data in Table III is typical of that obtained with the electronic counter-printer data acquisition system and was obtained from Sample No. 1 (0.030-in. thick), which was tested in methyl alcohol. This data is plotted in Figure 19, and illustrates the SWAT system sensitivity and the detailed information that can be obtained on crack growth in laboratory test specimens. Figure 19 also shows the cumulative stress-wave count for Specimen No. 1, which failed after approximately 15 minutes of exposure to methyl alcohol at an applied stress intensity of 35.4 ksi-in.$^{1/2}$. From the plot of the cumulative count, it can be seen that there are distinct changes in slope before the final drastic change at the onset of instability. The zero-slope portions of the cumulative-count curve are consistent with the zero count-rate (SWE/time) observations. The peaks in SWE/time corresponding to the rising portions of the cumulative-count curve may be either noise (detected because of the high sensitivity of the system), or crack-induced stress waves. However, these peaks in count rate are easily distinguishable from the increasing count rate and exponential cumulative count associated with failure; observation of the data on an oscilloscope would also distinguish crack-induced stress waves from noise. The point (a) in time corresponding to the rapid increase in count rate and cumulative count is taken to be the onset of detectable crack growth by SWE and provides sufficient time to terminate testing or vessel pressurization prior to failure.

Figures 15A and B, 16A and B, and 17 show SWE data for specimens exposed to air (Figure 15A and B) and inhibited water (Figures 16A and B, and 17); neither slow crack growth nor specimen fracture occurred during the hold periods. Each of the two specimens was held for about 1100 minutes at $K_I/K_{Ic} = 0.92$ without failure. From Figures 15B and 16B, it is evident that there is a constant slope in the curve of cumulative SWE count versus time at hold indicating background noise rather than SWE from crack growth was being counted. There is also no indication of slow crack growth

in the macrographs shown in Figures 8 and 9 for specimens exposed to air and inhibited water, confirming the stress-wave-emission data. The first part of Figure 17 was collected from data run during the day when adjacent laboratory, machine shop, and weld shop noises were characteristic of normal operating conditions. The drop in count rate toward the end of the test represents data obtained early in the morning before the laboratory, machine shop and weld shop were in operation.

As indicated previously, the random nature of this background noise could easily be distinguished from the SWE associated with flaw growth at a single source through the triangulation capability of a real time SWAT system; observation of the signals on an oscilloscope during the test could be similarly employed to distinguish between the two wave forms.

Figures 18 through 21 illustrate typical stress-wave emission data for specimens exposed to a methyl alcohol environment, indicating a markedly different behavior from air and inhibited water. In each test with a methyl alcohol environment, there was a positive indication of environmentally induced slow crack growth, as evidenced by stress-wave emission. From Figures 18 through 21 it is evident that there is a critical stress emission rate preceding failure. The cumulative-count plots illustrate how crack growth may be monitored by observing the change in the slope of the curves. In all instances, there is an increase in slope from a relatively constant value to an exponential slope which is a precursor to failure.

In the plots of stress-wave data for the methyl alcohol tests, the cumulative stress-wave count was plotted versus exposure time at constant load.* Figure 18 shows the cumulative stress-wave count for

*While the test specimens were held under constant load in the methyl alcohol environment, stress-corrosion cracking resulted in an increasing stress intensity factory.

IV, E, Discussion of Results (cont.)

Specimen No. 6 (0.030-in.-thick), which failed after approximately 23 minutes of exposure to methyl alcohol at an initial applied stress intensity of 24.3 ksi-in.$^{1/2}$ (80 ksi gross stress). Note that in this specimen, there appears to be a more or less linear increase in cumulative SWE count (a to b) followed by an increasing rate from b to failure. If a monitoring system were used to differentiate the stress-wave count with respect to time, the changing slope could be used as a precursor of crack instability. This curve indicates an increasing rate of stress-corrosion cracking starting after about 720 seconds (12 minutes) of exposure which could also be the primary incubation time at this stress intensity level.

Figure 20 shows the cumulative stress-wave count for Specimen No. 6 (0.060-in.-thick), which failed after approximately 165 minutes of exposure to methyl alcohol at an initial applied stress intensity of 27.2 ksi-in.$^{1/2}$ (67 ksi gross stress). Note from this plot that there appears to be two rates of increase in the cumulative count; at a to b, c to d, e to f, and g to h there is one slope, and a greater slope in between these increments. At c there appears to have been a pop-in; note that the plot of SWE/time versus hold time also indicates a larger-than-average increase in count rate at approximately 90 minutes.

From the standpoint of stress-wave emission characterization, the final instability was similar for all three environments since in each an increasing stress-wave-emission count rate and an increasing stress-wave amplitude was observed as failure was approached. The increased count rate is shown in Figures 18 through 21 for failure in the methyl alcohol environment. Figure 13 also shows this effect and the accompaning increased SWE amplitude which was observed immediately prior to failure during hold in the methyl alcohol environment and rising load in the air and inhibited water environments.

IV, E, Discussion of Results (cont.)

b. Comparison with SWE Data from Previous SPS Pressure Vessel Tanks

The SWAT system previously used during the SPS fuel tank test provided a full-scale output for an acceleration (g) level of 0.3g. Resolution to one-tenth of the 0.3g value or a discernment of 0.03g could readily be accomplished. No filtering was performed either prior to recording or during playback of the test data. Maximum available charge amplifier gain was 500:1.

In the present program, detection of stress-wave emissions from crack growth of titanium in methanol was accomplished with a total system gain of approximately 64000:1. Full-scale output was obtained for an acceleration (g) level of 0.00225g's. Minimum resolution was approximately 0.00015g. All data obtained was high pass filtered at 20 kiloHertz. Under prescribed test planning, these sensitivities should be obtainable during pressure vessel tests.

In verification of the increased sensitivity required to detect the small amplitude stress-wave emissions, the data tapes recorded during the SPS fuel tank test were reviewed. Data from the four sensors nearest the failure region were analyzed in a variety of ways. In one method, the data was visually observed on an oscilloscope as it was played back through a filter; in another way, the data was rerecorded through a light beam galvanometer and oscillographic recording system. Stress-wave emissions were also counted through use of the counting system previously described and used in this program.

In each instance, the following results were obtained:

IV, E, Discussion of Results (cont.)

(1) The resolution of stress-wave emissions detected during the test was considerably improved.

(2) The total number of SWEs detected was actually much greater than previously reported. A portion of these SWE may also, however, have originated from adhesive cracking. No attempt was made during this program to triangulate to their origin.

(3) The number of stress waves detected by the sensor on the forward head, the failure origin, and the nearest adjacent sensor were higher in count than at the next two sensor locations. For example, at sensor location No. 1 (on forward head nearest failure origin) and at sensor location No. 2 (nearest to forward head on the chamber cylinder) the stress-wave count through the pressure hold was 90 and 86, respectively. At more remote sensor positions three and four, the SWE count was 54 and 37, respectively.

Thus more stress-wave emissions of small amplitude were occurring in the region about sensor number one where failure occurred than at any other location on the SPS fuel tank. These stress waves were not large enough to be detected at more remote sensor positions with the system sensitivity in use at that time. However, with the new SWAT capabilities, in such major areas as sensor attachment techniques, sensitivity amplification, filtering and noise reduction, it is possible to increase the resolution of the SWE data both in real-time during testing and during data playback.

4. Application to Pressure Vessel Integrity

The purpose of both nondestructive inspection and hydrotest is to provide a high degree of assurance that the pressure vessel will not fail during service. The success of both procedures, however, is based on the

premise that each will assure that no defects larger than a given size are present in the vessel as it enters service. The specified size is based on a knowledge of the working stresses, the yield strength of the material, and the fracture toughness of the material; these facts permit calculation of the size of flaw that will be dangerous to the structure or tankage.

In service where an adverse environment is involved, the threshold stress intensity for subcritical cracking (K_{Iscc}) rather than the critical stress intensity, becomes the basis for calculating the dangerous flaw size. In air and the inhibited water investigated in this study, the threshold stress intensity factor was approximately 90% of K_{Ic}. For periods of up to 18 hours, there was no evidence of slow crack growth. The following calculated values of critical flaw size are based on a threshold stress intensity level of 0.9 K_{Ic} or 42.5 ksi-in.$^{1/2}$.

CRITICAL CRACK DEPTH (IN.) FOR AIR AND INHIBITED WATER

$K_{Ii}/K_{Ic} = 0.9$ ($K_{Ii} = 42.5$ ksi-in.$^{1/2}$)

Working Stress, ksi	Crack Shape (a/2c) 0.1	0.3	0.5
100	0.049	0.074	0.113
125	0.029	0.045	0.082
150	0.022	0.030	0.051

In methyl alcohol, the threshold level was not determined; at no time was the applied stress intensity level (K_{Ii}) low enough to eliminate subcritical crack growth in the hold periods investigated. Figures 20 and 21 indicate that significant slow crack growth began in the 0.060-in.-thick material after approximately 90 minutes of exposure to methyl alcohol at an applied stress intensity level of approximately 0.6 K_{Ic}. In the 0.030-in.-thick material, the slow crack growth was observed after approximately 10 minutes

of exposure to methyl alcohol (see Figures 18 and 19). Thus, for service involving less than 10 minutes of exposure to methyl alcohol, at an applied stress intensity level of 0.6 K_{Ic} (26.5 ksi-in.$^{1/2}$) the calculated values of critical flaw size would be as follows:

CRITICAL CRACK DEPTH (IN.) FOR METHYL ALCOHOL

$K_{Ii}/K_{Ic} = 0.6$ (K_{Ii} = 26.5 ksi-in.$^{1/2}$)

Working Stress, ksi	Crack Shape (a/2c) 0.1	0.3	0.5
100	0.014	0.027	0.043
125	0.012	0.014	0.023
150	0.008	0.010	0.014

the K_{Ii} values employed in the above calculations of critical crack depth were based on the initiation of subcritical crack growth rather than time to failure. However, it is common practice to base such calculations on time-to-failure measurements obtained for "practical" observation periods of less than a week (often less than twenty-four hours). The latter approach is obviously arbitrary and may be highly unconservative - after a week or any other arbitrary observation period, the specimen may not have failed, but slow crack growth may, nevertheless, be continuing and go undetected in the absence of a test method such as SWAT.

In a pressure vessel, subcritical slow crack growth can occur from small surface flaws present following manufacturing which pass undetected during subsequent nondestructive inspection or hydrotest. For example, if the inner-diameter surface of a pressure vessel were to have tool marks left from the finish-machining operation, it would be virtually impossible to detect the shallow surface flaws indicated in the above tabulations by conventional nondestructive inspection techniques. In hydrotest, such flaws may increase in

size but not sufficiently to result in failure. However, during subsequent long-time service, failure may occur because of slow crack growth even though the vessel passed hydrotest at a higher stress level.

In view of the above problems, it is considered highly desirable to employ SWAT as a supplementary nondestructive inspection technique both during laboratory investigations to generate reliable K_{Iscc} data and during hydrotest to determine the occurrence and location of flaw growth which may otherwise go undetected and result in subsequent service failures.

V. CONCLUSIONS

A. Sensor attachment techniques have been successfully developed and demonstrated which overcome previous bonding-agent problems encountered during the hydrotest of an Apollo SPS tank.

B. The system sensitivity required to detect stress-wave emissions from subcritical crack growth in thin walled (0.030 and 0.060-in.) 6Al-4V titanium alloy has been successfully achieved and demonstrated in air, distilled water inhibited with sodium dichromate (500 ppm), and methyl alcohol environments. Verification of adequate SWAT-system sensitivity was made through analysis of stress-wave emission data from a previous Apollo SPS-tank hydroburst.

C. Critical stress intensity (K_{Ic}) values of 43.5 ksi-in.$^{1/2}$ and 45.9 ksi-in.$^{1/2}$ were obtained, respectively, for the 0.030 and 0.060-in.-thick Ti-6Al-4V material evaluated in this study. These values compare well with the 44 ksi-in.$^{1/2}$ value obtained by NASA for the same 0.060-in.-thick material.

D. Air and distilled water inhibited with sodium dichromate (500 ppm) environments did not produce slow crack growth or failure during hold periods of up to 18 hours at applied stress intensity values of up to 0.92 K_{Ic}. This observation was verified both by the stress-wave emission data and by examination of the fracture surfaces.

E. In methyl alcohol, slow crack growth and failure always occurred during hold, with the time to failure dependent on the applied stress intensity. The K_{Iscc} for Ti-6Al-4V alloy in a methyl-alcohol environment was below 26.5 ksi-in.$^{1/2}$ (0.6 K_{Ic}), which was the lowest initial applied stress intensity investigated.

V, Conclusions (cont.)

F. The stress-wave emission characteristics which can be used as precursors of failure were the same for all environments investigated; these are: (1) the rate of occurrence, (2) the cumulative count, and (3) the amplitude of stress-wave emissions, all of which increased significantly as failure was approached.

G. In air and inhibited water, no significant SWE were observed under sustained load for hold periods of up to 18 hours. This was consistent with the fact that there was neither evidence of slow crack growth in the fracture surfaces nor failure during the hold periods. Failure during subsequent rising load was detected by monitoring the stress-wave emissions occurring and was attended by increased stress-wave rate of occurrence and amplitude.

H. In methyl alcohol, SWE indicative of the subcritical crack growth were observed during the holding periods and increased both in rate of occurrence and amplitude as failure approached.

I. The interval between the onset of detectable crack growth as shown by the stress-wave emission data and actual failure varied as a function of environment and applied stress intensity; in all instances, this time interval was sufficient to terminate the pressurizing cycle in a hydrotest prior to failure.

J. The stress-wave analysis technique should be employed as a method of detecting and locating the occurrence of subcritical crack growth during proof testing of critical tankage and during laboratory investigations of the threshold stress intensity level for subcritical crack growth (K_{Iscc}) and/or slow-crack-growth mechanisms. The need for SWAT is particularly acute in the proof testing of pressure vessels where past experience has shown that subcritical crack growth may occur without producing failure, and then cause failure even at lower service stresses due to additional, environmentally induced slow crack growth during long periods of service.

VI. RECOMMENDATIONS

A. The SWAT sensor attachment techniques and system sensitivity criteria evolved during this program should be verified through the hydrotest of an Apollo Service Propulsion System (or similar thin-walled) pressure vessel. A mobile SWAT instrumentation van is presently available for this purpose and would demonstrate the application of criteria evolved through this study under actual hydrotest conditions.

B. Subsequently, a SWAT instrumentation system should be designed specifically to meet Apollo requirements. The design should be suitable for interfacing with other NASA materials and/or component test instrumentation such as currently available computer, data readout and hydrotest facilities.

C. Stress-wave emission data should be obtained on a routine basis during materials test programs, particularly those investigating slow crack growth where it would be possible to obtain stress wave emission characterization data for application during subsequent component hydrotest and/or in-service monitoring. Such data would be useful during the materials study by determining the occurrence of subcritical crack growth where no other technique is available (such as during the testing of part-through-crack tensile) and in providing a more basic understanding of the mechanisms of slow crack growth.

D. Investigations should be conducted to investigate the interactions of multiple flaws on titanium fracture. Such studies could be employed using PTC-tensile specimens of both parent metal and welds and using SWAT as a real-time technique to indicate the load and test time at which interactions occur. This information would be useful in assessing the integrity of such critical pressure vessel areas as welds where multiple porosity often occurs, and in determining associated accept/reject criteria.

VI, Recommendations (cont.)

E. Tests to establish the threshold K_{Iscc} value for critical Apollo material-environment combinations should be performed using SWAT as a means of detecting the occurrence of subcritical crack growth. This would include a continuation of the methyl alcohol tests initiated in this program. Currently, the K_{Iscc} values are obtained on the basis of plots of applied stress intensity vs time to failure where the latter measurements usually are based on practical observation periods of less than a week. This is obviously arbitrary and may be highly unconservative - after a week or any other arbitrary observation period, the specimen may not have failed, but slow crack growth may, nevertheless, be continuing and go undetected in the absence of a method such as SWAT.

REFERENCES

1. C. E. Hartbower and P. P. Crimmins, "Fracture of Structural Metals as Related to Pressure-Vessel Integrity and In-Service Monitoring", AIAA Paper 68-501 presented at the ICRPG/AIAA 3rd Solid Propulsion Conference, Atlantic City, June 4-6, 1968.

2. A. T. Green, C. S. Lockman, S. J. Brown, R. K. Steele, "Feasibility Study of Acoustic Depressurization System", NASA CR 55472, March 1966.

3. R. K. Steele, A. T. Green, C. S. Lockman, "Acoustic Verification of Structural Integrity of Polaris Chambers", Society of Plastics Engrs 20th Meeting, Atlantic City, N.J., January 1964.

4. Pressure Testing of AFRM-017 Service Propulsion System Fuel Tank Utilizing Aerojet-General Corporation's Stress-Wave Analysis Technique (SWAT), Report NAS 9-6766-003, May 1967, prepared by Aerojet-General Corp. for NASA, MSC, Houston, Texas, under Contract NAS 9-6766.

5. G. K. Tasanen and B. M. Wigle, "Accelerometer Mounting and Data Integrity", Sound and Vibration, Nov. 1967.

6. G. Stathopoulos, "Effect of Mounting on Accelerometer Response", Electronic Industries, May 1962.

7. Technical Data Book S-3, RTV Silicone Rubber, General Electric, Waterford, N.Y.

8. G. R. Irwin, "Crack Extension Force for a Part-Through-Crack in a Plate", Journal of Applied Mechanics, Vol 84E No. 4, Dec 1962.

9. Kobayashi, A. S., Boeing Structural Development Research Memorandum SDRM 16.

10. Smith, F. W., Boeing Structural Development Research Memorandum SDRM 17.

11. Mechanisms of Slow Crack Growth in High-Strength Steels, C. E. Hartbower, W. W. Gerberich, and P. P. Crimmins, AFML-TR-67-26, Vol 1, Feb 1967.

12. W. F. Brown, Jr., and J. E. Srawley, "Plane-Strain Crack Toughness Testing High-Strength Metallic Materials", ASTM STP No. 410, Dec. 1966.

13. Tensile Properties and Fracture Toughness of 6Al-4V Titanium, C. E. Hartbower, W. G. Reuter, and P. P. Crimmins, AFML-TR-68-163, Vol I, Appendix B, p.91, Sept 1968.

14. C. E. Hartbower, Minutes of ASTM E-24 Subcommittee III Meeting, on Medium Strength High-Toughness Materials, Atlanta, Georgia, Sept 30, 1968.